



A Comparative Study of Geothermal Pipeline Route Selection Methods with Visual Effects Optimization

Sigurjón Norberg Kjærnested



**Faculty of Industrial Engineering,
Mechanical Engineering and
Computer Science
University of Iceland**

A Comparative Study of Geothermal Pipeline Route Selection Methods with Visual Effects Optimization

Sigurjón Norberg Kjærnested

60 ECTS thesis submitted in partial fulfillment of a
Magister Scientiarum degree in Mechanical Engineering

Advisors

Magnús Þór Jónsson

Halldór Pálsson

Faculty Representative

Tómas Philip Rúnarsson

Faculty of Industrial Engineering, Mechanical Engineering and Computer
Science

School of Engineering and Natural Sciences

University of Iceland

Reykjavik, Oktober 2011

A comparative study of geothermal pipeline route selection methods with visual effects optimization
60 ECTS thesis submitted in partial fulfillment of a Magister Scientiarum degree in
Mechanical Engineering

Copyright © 2011 Sigurjón Norberg Kjærnested
All rights reserved

Faculty of Industrial Engineering, Mechanical Engineering and Computer Science
School of Engineering and Natural Sciences
University of Iceland
Hjardarhagi 2-6
107, Reykjavik
Iceland

Telephone: 525 4700

Bibliographic information:
Printing: Háskólaprent
Reykjavik, Iceland, Oktober 2011.

Printing: Háskólaprent
Reykjavik, Iceland, Oktober 2011

Abstract

The objective of this study is to develop a methodology and to create a tool for use in geothermal pipeline route selection. Special emphasis is placed on the method minimizing the visual effects of the pipeline. Two different methods for route selection are presented.

In the first method, distance transform algorithms are utilized. First a method is presented to rank each point, in a digital elevation model representing the topography in question, based on visibility with regards to roads, buildings and public areas. Then a new extension to variable topography distance transform algorithms is employed to obtain the optimal path. The second method uses a non-dominated sorting genetic algorithm to obtain the optimal path with regards to first of all visual effects and pipeline length and second of all visual effects and pressure drop. This method also works with the distance transform ranking method presented in this study. A new method to generate the initial genetic algorithm population based on visual effects and pipeline length constraints is presented. The constraint's included in both methods are maximum allowable pipeline incline and inaccessible areas.

The methods are implemented for the Hverahlíð geothermal area in Iceland. The visual effects and length of the routes recommended by the methods are compared to each other, those of the shortest possible route and the route proposed in the original planning for the geothermal area. Both the methods presented by this study are effective in obtaining pipeline routes with significantly less visual effects than conventionally designed pipeline routes. In particular the distance transform based method offers a good, functional way to design pipeline routes with regards to minimal visual impact without the route length becoming too long.

Útdráttur

Markmiðið með þessari rannsókn er að þróa aðferðafræði og búa til verkfæri fyrir hönnun á leiðum píþna á jarðvarmasvæðum. Sérstök áhersla er lögð á að aðferðin takmarki sjónræn áhrif píþnanna. Tvær mismunandi aðferðir fyrir leiðarval eru kynntar.

Í fyrstu aðferðinni eru notuð fjarlægðar-umbreytingar algrím. Fyrst er kynnt aðferð sem að gefur hverjum punkti, í stafrænu hæðarlíkani af landslagi, einkunn byggt á hversu vel sá punktur sést frá t.d vegum, byggingum og ferðamannasvæðum. Síðan er ný viðbót við fjarlægðar-umbreytingar algrím notuð til að finna bestu leiðina. Önnur aðferðin notar genetísk algrím til að finna bestu leiðina með tilliti til í fyrsta lagi sjónrænna áhrifa og lengdar leiðarinnar og í öðru lagi með tilliti til sjónrænna áhrifa og þrýstifalls í píþunni. Seinni aðferðin metur sjónræn áhrif á sama hátt og sú fyrri. Ný aðferð er kynnt til að búa til upphaflegu einstaklingana fyrir genetísk algrím, með tilliti til skorða á sjónrænum áhrifum og lengdar píþu. Aðrar skorður sem báðar aðferðir taka tillit til eru hámarkshalli píþu og óaðgengileg svæði.

Aðferðirnar eru báðar prófaðar á jarðvarmasvæðinu Hverahlíð á Íslandi. Sjónræn áhrif og lengd leiðanna eru borin saman við hvor aðra, stystu mögulegu leið og þá leið sem að upphaflega var ákveðin í skipulagi svæðisins. Báðar aðferðirnar sem að kynntar eru í þessari rannsókn eru árangursríkar í að hanna leiðir fyrri píþur með töluvert minni sjónrænum áhrifum en leiðir hannaðar á hefðbundinn hátt. Sérlega býður aðferðin byggð á fjarlægðar-umbreytingar algrímum upp á góða og nothæfa leið til að hanna leiðir fyrir píþur á jarðvarmasvæðum með tilliti til þess að takmarka sjónræn áhrif, án þess að auka um of lengd leiðarinnar.

Table of Contents

| | |
|--|-----------|
| Abbreviations..... | xi |
| Acknowledgements | xv |
| 1 Introduction..... | 1 |
| 1.1 Motivation | 1 |
| 1.2 Previous work and contribution | 1 |
| 1.3 Overview | 2 |
| 2 Present methods | 3 |
| 2.1 Distance transforms | 3 |
| 2.1.1 Chamfer distance transforms | 4 |
| 2.1.2 Digital elevation models | 7 |
| 2.1.3 Variable topography distance transforms | 9 |
| 2.1.4 Multiple weight distance transforms..... | 11 |
| 2.1.5 Non-accessible areas and distance transforms..... | 12 |
| 2.1.6 Optimal route with distance transform algorithms | 14 |
| 2.2 Genetic algorithms | 15 |
| 2.2.1 Basic principles | 15 |
| 2.2.2 Multi-objective optimization and pareto genetic algorithms | 17 |
| 2.2.3 Non dominated sorting genetic algorithm..... | 18 |
| 2.2.4 Non-dominated sorting genetic algorithm II..... | 19 |
| 2.3 Pressure drop of two-phase flow in pipelines | 20 |
| 3 Adjustment of methods for route optimization..... | 25 |
| 3.1 Distance transform visual effects ranking | 25 |
| 3.2 Distance transform based method | 29 |
| 3.2.1 Constrained multiple weight distance transforms..... | 29 |
| 3.2.2 Multi-objective least cost distance transforms..... | 31 |
| 3.2.3 GA modification of DT route | 32 |
| 3.2.4 Summary of distance transform based method..... | 35 |
| 3.3 Genetic algorithm based method..... | 35 |
| 3.3.1 Motivation..... | 35 |
| 3.3.2 Genetic algorithm population generation using visual effects ranking and inaccessible areas | 36 |
| 3.3.3 Individuals and genetic operators | 37 |
| 3.3.4 Objective and penalty functions..... | 38 |
| 4 Results | 41 |
| 4.1 Geothermal area features and case study details | 41 |

| | | |
|----------|---|-----------|
| 4.2 | Distance transform based method - results | 42 |
| 4.3 | Genetic algorithm based method – results | 45 |
| 4.4 | Comparison of method performance..... | 47 |
| 4.5 | MLCDT with and additional cost function | 48 |
| 4.6 | Inclusion of a pressure drop objective function | 50 |
| 5 | Conclusions and future work | 53 |
| | References | 55 |

Abbreviations

| Symbol | Description | Symbol | Description |
|-----------------------|---|-----------------------|---|
| d_k | Grid point value of k-th element in a chamfer mask | n_i | Individual domination count |
| $LDM(k)$ | Local distance metric | S_i | Individual domination set |
| d_0 | Current value of grid point at center of chamfer mask | N | Population size |
| DEM_k | Height of digital elevation model in the grid point corresponding to the k-th element of the mask | $NumObs$ | Number of observation points |
| DEM_0 | Height of digital elevation model in the grid point corresponding to the center element of the mask | $rank(k)$ | Visual effects rank of grid point with regards to observation point k |
| MSlope | Maximum allowed slope | $TotalRank(i, j)$ | Total visual effects rank of grid point (i,j) |
| A_i | Set number i | tol | Defined tolerance for visual effects behind grid point |
| $DT(A_i)$ | Distance transform on set A_i | x' | Pareto optimal vector |
| k_i | Relative weight of set A_i | n | Number of objective functions in a pareto optimal set |
| $cost_n(x, y)$ | Value of cost function n at (x,y) | σ | Surface tension |
| \vec{x} | Vector of design variables | d_{ij} | Sharing parameter |
| $f_i(\vec{x})$ | i-th objective function | $C(d_{ij})$ | Sharing function value for two individuals in the same front |
| $g_j(\vec{x})$ | j-th constraint function | w_i | i-th weight coefficient |
| σ_{share} | Sharing parameter | ΔP_{total} | Total pressure drop |
| ΔP_{static} | Static pressure drop | $\Delta P_{friction}$ | Frictional pressure drop |
| $\Delta P_{momentum}$ | Momentum pressure drop | ΔP_{bends} | Pressure drop in bends |
| A | Pipeline cross sectional area | \dot{m} | Mass flow rate |
| A_g | Cross sectional area of gas phase | \dot{m}_v | Mass velocity |

| | | | |
|------------------|--|-------------------------------------|--|
| ϵ | Void fraction | ρ_H | Homogeneous density |
| ρ_l | Liquid phase density | ρ_g | Gas phase density |
| x | Steam quality | Re | Reynolds number |
| μ_l | Liquid phase dynamic viscosity | μ_l | Gas phase dynamic viscosity |
| d_i | Pipeline inner diameter | \bar{V}_f | Liquid phase velocity |
| \bar{V} | Average velocity of equivalent single phase flow | μ_{tp} | Two phase dynamic viscosity |
| f_{tp} | Two phase friction coefficient | AC | Acceleration correction factor |
| p | Pressure | \dot{m}_g | Mass flow rate of gas phase |
| n_b | Number of bends | h_b | Bend equal length |
| n_{eu} | Number of expansion units | h_{eu} | Expansion unit equal length |
| n_c | Number of connections | h_c | Connection equal length |
| n_v | Number of valves | h_v | Valve equal length |
| φ_b^2 | Two phase multiplier for bends | φ_c^2 | Two phase multiplier for connections |
| φ_{eu}^2 | Two phase multiplier for expansion units | φ_v^2 | Two phase multiplier for valves |
| r | Bend radius | $\left. \frac{dP}{dz} \right _{lb}$ | Single phase bend pressure drop |
| DT | Distance transform | DEM | Digital elevation model |
| VTDT | Variable topography distance transform | LCDT | Least cost distance transform |
| MWDT | Multiple weight distance transform | CMWDT | Constrained multiple weight distance transform |
| MLCDT | Multi-objective least cost distance transform | GA | Genetic algorithm |
| MOO | Multi-objective optimization | NSGA II | The non-dominated sorting genetic algorithm II |
| NSGA | A non-dominated sorting genetic algorithm | PI | Performance index |

| | | |
|-----|----------------------------|--------------|
| MOP | Multi-objective problem | optimization |
|-----|----------------------------|--------------|

Acknowledgements

I would like to express my sincere thanks to my thesis advisor Dr. Magnús Þór Jónsson for his great guidance, help and support throughout this process. I would also like to thank Dr. Halldór Pálsson for his great guidance and help.

Special thanks also go out to the Geothermal Research Group (GEORG) for financial support. I also give acknowledgement and thanks to the company Reykjavík Energy for supplying all the information necessary for the Hverahlíð geothermal area case studies.

Finally I would like to thank my fiancée and my parents for their great patience and support.

1 Introduction

1.1 Motivation

Route selection in geothermal areas in Iceland is a topic of growing importance. The visual effects of pipelines in Icelandic geothermal areas are a debated topic and demands for burying pipelines to eliminate their visual effects are growing louder, both from the public at large and the government. This would however significantly increase the costs of geothermal power plants, rendering less the feasibility of utilization of new geothermal areas. Therefore it is desired to obtain a route design method that minimizes the visual effects of a pipeline while also addressing other concerns regarding geothermal pipeline route design. This is in essence the main objective of this study, to construct a method for pipeline route design that minimizes the visual effects of the pipeline.

1.2 Previous work and contribution

Route optimization is a topic that has been studied extensively and algorithms designed to obtain the shortest or least-cost path are readily available. None of these methods have however been adapted to the specific problem of obtaining the least-visual effects route for pipelines. In this study two classes of algorithms are used and adapted to solve this problem, distance transform algorithms and non-dominated sorting genetic algorithms. Distance transform (DT) algorithms have been shown (Smith, 2005) to be very effective at obtaining the shortest route in a very computationally effective way. A DT algorithm also has the useful property of registering the shortest path from each point in the grid to the closest object point and this property is used (as will be presented below) in the visual effects ranking method. Genetic algorithms have been extensively used in recent years with good results for multi-objective optimization problems (Cheng & Li, 1997). For this reason a multi-objective genetic algorithm is adapted for the second method of this study.

The specific DT used in the first method of this study is the variable topography distance transform algorithm (VTDT). The VTDT was introduced by De Smith (2005). The VTDT has been used by Kristinsson (2005) to obtain the shortest route for geothermal pipelines, showing good results. De Smith (2004) also introduced the Multiple Weight Distance Transforms (MWDT). The use of the MWDT for separator selection was suggested by Kristinsson (2005). The MWDT is extended in this study to include constraints and inaccessible areas and is utilized to obtain the optimal location for separators and power plants.

The first method of this study extends the work of Kristinsson (2005) and de Smith (2005) first of all to include visual effects optimization and second of all the inclusion of multiple cost functions is examined. The main innovation of this study is the method of ranking visual effects and then the optimization with the two different methods with regards to visual effects. The visual effects ranking method is used by both the methods of this study. This first method presented, represents a complete tool for the optimization of pipeline

routes in geothermal areas with regards to minimizing the visual effects and includes the selection of power plant, pipeline gathering point and separator sites.

The second method presented in this study uses the Non-dominated sorting genetic algorithm II (Deb, Agrawal, Pratap, & Meyarivan, 2002). The algorithm used in this study uses all the principles of the NSGA II with some additions and adjustments, as will be further discussed below. A new method of generating the initial population based on visual effects and pipeline length is proposed in this study, as an extension to the NSGA II for the particular problem of pipeline routing. A simple GA is also used for both methods to optimize the inclusion of expansion units. The second method includes optimization with regards to pressure drop, visual effects and route length.

In the past few years many evolutionary multi-objective algorithms that obtain solutions on the pareto-optimal front have been proposed but the NSGA II has been shown to be less computationally intensive and perform better with regards to obtaining well distributed solutions over the pareto front (Deb, Agrawal, Pratap, & Meyarivan, 2002). Therefore it was chosen as the basis for the second method of this study.

To summarize the innovations to the presently used methods in this study include, for the first method, adjustments to the distance transform algorithms (in the form of the MLCDT covered below) and a new distance transform based visual effects ranking method. The second method also utilizes the distance transform visual effects ranking method along with the NSGA II algorithm, which has not been adapted before to the problem of pipeline route optimization.

1.3 Overview

Chapter two provides background on the present methods used in this study. First of all the methods used for route selection in the geothermal industry and methods used for pipeline route selection in general are reviewed. Then introductions to distance transform algorithms and non-dominated sorting genetic algorithms are provided. The final part of the second chapter covers pressure drop in two phase pipelines. In chapter three adjustments and additions to the present methods – all of the innovations of this study - are presented along with a new method of ranking points in a given topography, based on visual effects. In the fourth chapter the Hverahlíð geothermal area case study is presented and in the fifth chapter the conclusions of this study are discussed

2 Present methods

In the geothermal industry today mathematical optimization of the pipeline route is not common. The most common methods employed are ad hoc methods, with the design process largely manual. Often GIS based systems are employed for manual selection of pipeline routes. Throughout the design process the main goal is to keep the pipeline route as short as possible, to minimize costs and pressure drop. It is also important to minimize turns due to the extra costs they incur. Another important goal is to minimize incline, first of all to prevent undesirable flow regimes from forming (i.e slug flow conditions) and second of all due to pressure drop if the incline is upwards. Taken into account in the design process is the inclusion of expansion loops at regular intervals. Due to the high temperatures in geothermal pipelines, expansion loops are necessary at regular intervals. One of the main impetuses of this study is to optimize this process and provide an effective design-aid.

Recently it has been becoming more common to take the visual effects of pipelines into account in the design process. This has specifically been the case in Iceland, but to a lesser degree in other countries. Geothermal pipelines are relatively large and due to the inherent nature of geothermal fields, must often traverse great distances to reach the power plant. This is especially the case for re-injection pipelines. Due to the cooling effects re-injection has on the reservoir, it is often desired to re-inject the geothermal brine in the peripheral areas of the reservoir. Re-injection pipelines therefore at times need to travel great distances. Geothermal areas are often by their very nature thought of as worthy of protection and therefore it is desired to minimize the visual effects. Though this aspect is currently at times taken into account in the design process, it is not optimized.

Route optimization is a topic that has been studied extensively and a plethora of algorithms designed to obtain the shortest or least-cost path are available. This study does not offer a comprehensive state of the art of those methods but will touch on some of the most common of them. Linear programming methods have been popular (Gass, 1985) but many other optimization techniques have also been adapted to the problem. Metaheuristic algorithms have in recent years especially been used extensively. Genetic algorithms (Gopalakrishnan & Sooda, 2009), ant colony optimization (Bell & McMullen, 2004), simulated annealing (Gopalakrishnan & Sooda, 2009), particle swarm optimization (Yavuz, 2004) and harmony search (Geem, Lee, & Park, 2005) are examples of methods that have been used for vehicle routing techniques. Finally, as previously mentioned distance transform algorithms have been adapted to the problem (Kristinsson, 2005). In this study that method is modified and extended.

2.1 Distance transforms

A distance transform is an image processing algorithm for digital images. A standard DT works with a binary digital image that consists of object points and non-object points represented by black and white respectively in figure 2.1 below. At its simplest, for each non-object point in an image, a DT obtains the distance from that point to the closest object point. Any point in an image can be defined as an object point, they are simply a set of points from whom, for each point, it is desired to map the distance to the closest object point. An example is shown below. In the resulting matrix after a DT has been performed

on the image, each non-object grid point has a value corresponding to its distance to the closest the object point. This is depicted in figure 2.1. The ability to generate the distance isolines that can be clearly seen on the right in figure 2.1 is the most important property of distance transforms. It is from this property that the possibility of using DT's for route optimization arises.

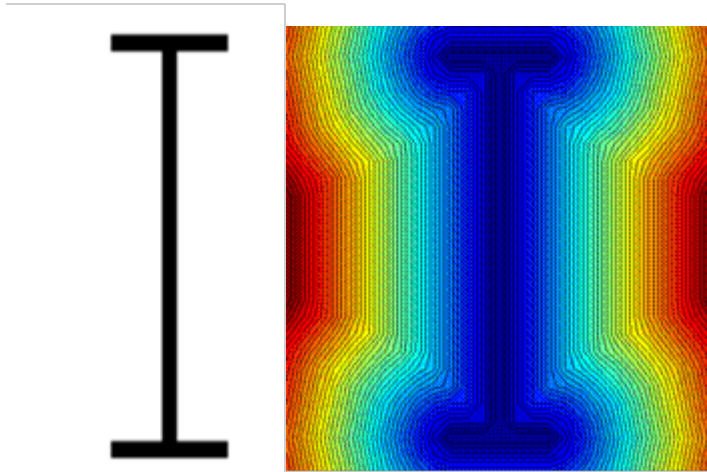


Figure 2.1: Example of a simple distance transform. The black pixels in image showing the letter „I“ on the left represent object points, all the other pixels in the image (the white pixels) represent pixels for whom the distance transform calculates the distance to the closest object point. The results of the distance transform, the distance isolines, are shown in the color image on the right where the scale is from dark blue – closest to object points- to dark red – furthest away from object points.

2.1.1 Chamfer distance transforms

When utilizing a distance transform algorithm it is straightforward to utilize exact Euclidian distances to generate the distance isolines. This is in essence a global operation and unless the digital picture is very small, calculating the exact Euclidian distances can be computationally intensive and inefficient, therefore it is more efficient to compute local distances and propagate them over the entire image to estimate the global distances (Smith, 2004). This is most commonly done by using chamfer metrics which estimate the distance from the target point to the cells in a local neighborhood. Most commonly 3x3, 5x5 or 9x9 chamfers are utilized with the computation being in a parallel or sequential manner as will be covered below. For computations in this study a 5x5 chamfer was utilized. The larger a chamfer is, the greater accuracy is achieved, but at the same time calculations become more computationally intensive. The 5x5 chamfer was deemed to offer a compromise between computational intensiveness and accuracy and was therefore chosen. Figures 2.2.1-3 depict 3x3, 5x5 and 9x9 chamfers respectively:

| | | |
|---|---|---|
| b | a | b |
| a | X | a |
| b | a | b |

Figure 2.2.1: 3x3 chamfer matrix that is used in a distance transform algorithm, the letters a-b represent the incremental distances in the chamfer matrix

| | | | | |
|----|---|----|---|----|
| 2b | c | 2a | c | 2b |
| C | b | a | b | C |
| 2a | a | X | a | 2a |
| C | b | a | b | C |
| 2b | c | 2a | c | 2b |

Figure 2.2.2: 5x5 chamfer matrix that is used in a distance transform algorithm, the letters a-c represent the incremental distances in the chamfer matrix

| | | | | | | |
|----|----|---|----|---|----|----|
| 3b | e | d | 3a | d | e | 3b |
| e | 2b | c | 2a | c | 2b | e |
| d | C | b | a | b | c | d |
| 3a | 2a | a | X | a | 2a | 3a |
| d | c | b | a | b | C | d |
| e | 2b | c | 2a | c | 2b | e |
| 3b | e | d | 3a | d | e | 3b |

Figure 2.2.3: 7x7 chamfer matrix that is used in a distance transform algorithm, the letters a-e represent the incremental distances in the chamfer matrix

When computing a distance transform on a digital image, the values of all the object points in the image are set to zero and the values of all other points are set to a very large number (f.a.e 999999). The next step is to place chamfer masks successively over each pixel in the image, which maps the value of the distance to the nearest object point to each grid point. Distance transforms can be computed in parallel or sequentially, in this study parallel calculations will be employed, with a forward and a backward mask placed over each pixel in the image and the local values in the mask computed. The algorithm is iterative and can require a large number of iterations (f.a.e 10-30 for the digital elevation model matrix used in the case study presented in chapter 4) to complete the distance transformation, depending on the matrix size. A forward and backward mask for 7x7 chamfers are depicted below in figures 2.3.1 and 2.3.2

| | | | | | | |
|----|----|---|----|---|----|----|
| 3b | e | d | 3a | d | e | 3b |
| e | 2b | c | 2a | c | 2b | e |
| d | c | b | a | b | c | d |
| 3a | 2a | a | X | | | |

Figure 2.3.1: Forward mask for parallel calculations in a distance transform algorithm utilizing a 7x7 chamfer matrix, the letters a-d represent the incremental distances in the chamfer matrix

| | | | | | | |
|----|----|---|----|---|----|----|
| | | | X | a | 2a | 3a |
| d | c | b | a | b | c | d |
| e | 2b | c | 2a | c | 2b | e |
| 3b | e | d | 3a | d | e | 3b |

Figure 1.3.2: Backward mask for parallel calculations in a distance transform algorithm utilizing a 7x7 chamfer matrix, the letters a-e represent the incremental distances in the chamfer matrix

The central function in a distance transfer algorithm is the following (Bellman's equation):

$$d_0 = \min(d_k + LDM(k), d_0) \quad 2.1)$$

Where d_k is the grid point value of the k-th element in a chamfer mask, LDM(k) is the local distance metric and d_0 the current value of the grid point at the center of the chamfer mask. The algorithm places the masks in parallel on each pixel in an image. The result of employing a DT algorithm on a digital image is a matrix where all the elements have the value of the distance to the closest image pixel. An example of a sequential DT on a simple digital image is shown below in figures 2.4.1-3

| | | | | | | | | |
|-------|-------|-------|-------|-------|-------|-------|-------|-------|
| 99999 | 99999 | 99999 | 99999 | 99999 | 99999 | 99999 | 99999 | 99999 |
| 99999 | 99999 | 99999 | 99999 | 0 | 99999 | 99999 | 99999 | 99999 |
| 99999 | 99999 | 99999 | 99999 | 99999 | 99999 | 99999 | 99999 | 99999 |
| 99999 | 99999 | 99999 | 99999 | 99999 | 99999 | 99999 | 99999 | 99999 |
| 99999 | 99999 | 99999 | 99999 | 99999 | 99999 | 99999 | 99999 | 99999 |
| 99999 | 0 | 99999 | 99999 | 99999 | 99999 | 99999 | 0 | 99999 |
| 99999 | 99999 | 99999 | 99999 | 99999 | 99999 | 99999 | 99999 | 99999 |
| 99999 | 99999 | 99999 | 99999 | 99999 | 99999 | 99999 | 99999 | 99999 |
| 99999 | 99999 | 99999 | 99999 | 99999 | 99999 | 99999 | 99999 | 99999 |
| 99999 | 99999 | 99999 | 99999 | 0 | 99999 | 99999 | 99999 | 99999 |
| 99999 | 99999 | 99999 | 99999 | 99999 | 99999 | 99999 | 99999 | 99999 |

Figure 2.4.1: Example matrix for use in a distance transform example. Object points are represented by „0“ and all other grid points by „99999“. The results of using a distance transform algorithm on this matrix are shown in figures 2.4.2 and 2.4.3 respectively

| | | | | | | | | |
|-----|-----|-----|-----|-----|-----|-----|-----|-----|
| 4,2 | 3,2 | 2,2 | 1,4 | 1,0 | 1,4 | 2,2 | 3,2 | 4,2 |
| 3,9 | 3,0 | 2,0 | 1,0 | 0,0 | 1,0 | 2,0 | 3,0 | 3,9 |
| 3,2 | 3,0 | 2,2 | 1,4 | 1,0 | 1,4 | 2,2 | 3,0 | 3,2 |
| 2,2 | 2,0 | 2,2 | 2,2 | 2,0 | 2,2 | 2,2 | 2,0 | 2,2 |
| 1,4 | 1,0 | 1,4 | 2,2 | 3,0 | 2,2 | 1,4 | 1,0 | 1,4 |
| 1,0 | 0,0 | 1,0 | 2,0 | 3,0 | 2,0 | 1,0 | 0,0 | 1,0 |
| 1,4 | 1,0 | 1,4 | 2,2 | 3,0 | 2,2 | 1,4 | 1,0 | 1,4 |
| 2,2 | 2,0 | 2,2 | 2,2 | 2,0 | 2,2 | 2,2 | 2,0 | 2,2 |
| 3,2 | 3,0 | 2,2 | 1,4 | 1,0 | 1,4 | 2,2 | 3,0 | 3,2 |
| 3,9 | 3,0 | 2,0 | 1,0 | 0,0 | 1,0 | 2,0 | 3,0 | 3,9 |
| 4,2 | 3,2 | 2,2 | 1,4 | 1,0 | 1,4 | 2,2 | 3,2 | 4,2 |

Figure 2.4.2: Matrix showing results from using a distance transform algorithm on the example matrix shown in figure 2.4.1.

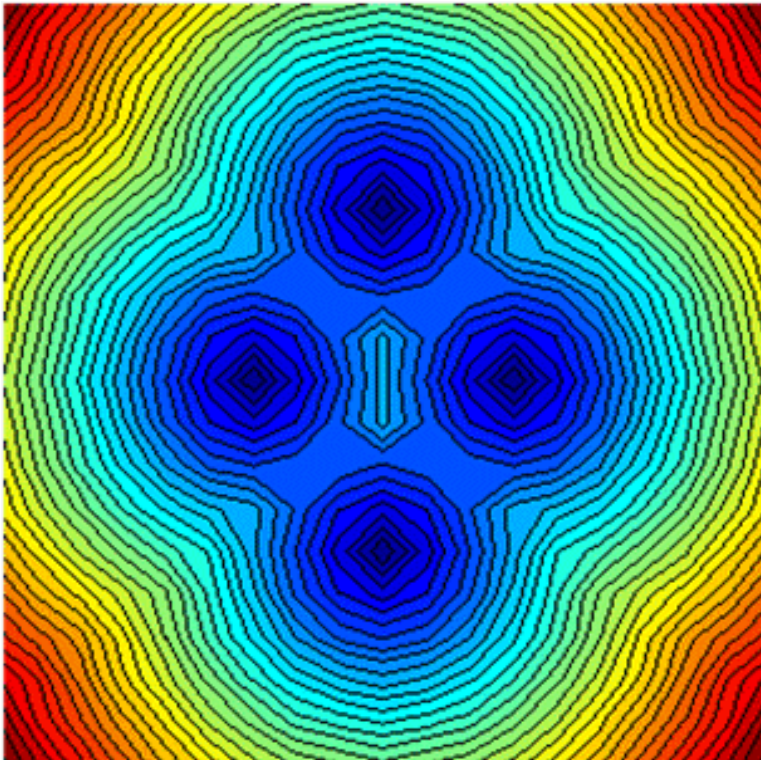


Figure 2.4.3: Visual representation of matrix showing results from using a distance transform algorithm on the example matrix shown in figure 2.4.1. The scale is from dark blue – closest to object points- to dark red – furthest away from object points.

2.1.2 Digital elevation models

A digital elevation model (DEM) is a digital representation of a given ground topography. DEM's are available for the majority of Icelandic topography with an accuracy of up to $0.25 m^2$. Each grid point in a digital elevation model matrix will have a value equal to (or proportional to) the height of the corresponding topography. An example of a DEM is

shown below in figure 2.5.2 which represents only a random part of the topography in figure 2.5.1 (the DEM corresponding to figure 2.5.1 is 500x500 grid points).

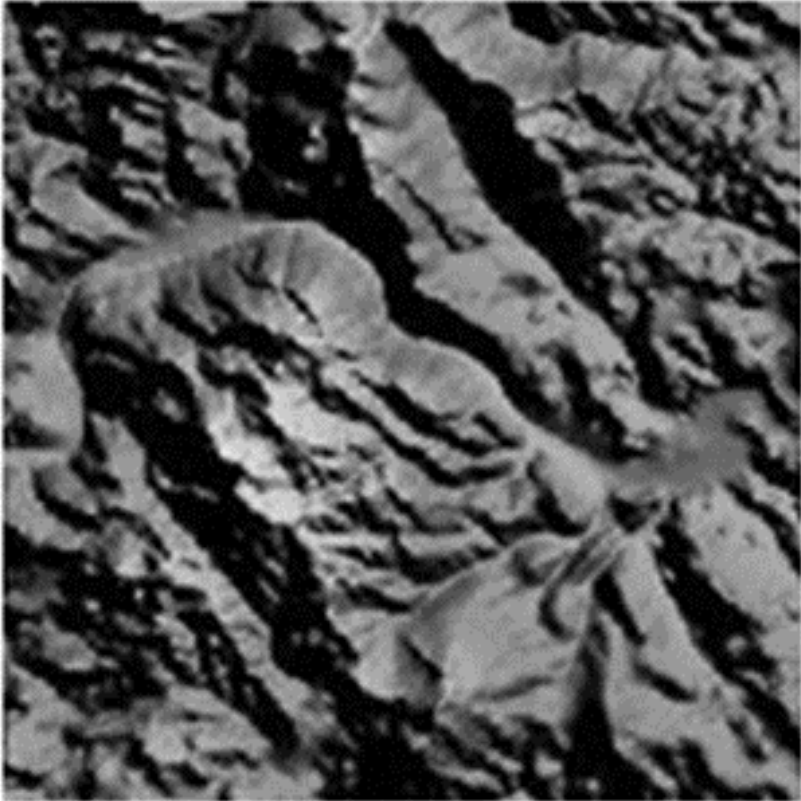


Figure 2.5.1: Example topography, digital elevation model of which is partially depicted in figure 2.5.2. The scale is from black – lowest elevation in this topography- to white – highest elevation in this topography.

| | | | | | | | | | | |
|-----|-----|-----|-----|----|----|-----|-----|-----|-----|-----|
| 154 | 99 | 75 | 82 | 67 | 73 | 81 | 88 | 100 | 122 | 127 |
| 102 | 104 | 76 | 88 | 61 | 57 | 86 | 98 | 104 | 111 | 118 |
| 69 | 103 | 68 | 50 | 74 | 30 | 64 | 92 | 107 | 102 | 113 |
| 77 | 76 | 107 | 128 | 76 | 17 | 60 | 92 | 111 | 102 | 113 |
| 84 | 82 | 99 | 99 | 18 | 29 | 63 | 86 | 107 | 103 | 117 |
| 64 | 83 | 76 | 76 | 32 | 28 | 67 | 85 | 116 | 126 | 143 |
| 52 | 88 | 83 | 33 | 28 | 42 | 102 | 109 | 108 | 130 | 147 |
| 45 | 104 | 86 | 26 | 14 | 37 | 110 | 138 | 100 | 127 | 135 |
| 21 | 55 | 89 | 30 | 46 | 73 | 105 | 119 | 119 | 173 | 157 |
| 33 | 17 | 64 | 37 | 60 | 55 | 64 | 102 | 143 | 165 | 176 |
| 101 | 19 | 19 | 26 | 28 | 53 | 34 | 121 | 171 | 160 | 178 |

Figure 2.5.2: Digital elevation model of a random part of figure 2.5.1. Each grid point has the value of the height at the corresponding topographical location.

2.1.3 Variable topography distance transforms

Variable topography distance transforms were introduced by Smith (2005). A VTDT algorithm offers a way to obtain the shortest path by using distance transforms on digital elevation models and introducing constraints by way of digital elevation models. 3-D landscapes are essentially open 2-D manifolds, which renders this possible (Smith, 2005). The VTDT algorithm incorporates slope constraints by assigning each cell a value from the corresponding digital elevation model. The slope distance is then calculated and if it exceeds the defined maximum slope a new value is not mapped to the grid point. The adjustment to the main function of the algorithm is as follows:

$$\text{slope} = \frac{\text{DEM}_k - \text{DEM}_0}{\text{LDM}(k)} \quad 2.2)$$

$$\text{if}(d_k + \text{LDM}(k) < d_0 \ \&\& \ \text{slope} < \text{MSlope})$$

$$\text{then: } d_0 = d_k + \text{LDM}(k) \quad 2.3)$$

Where DEM_k represents the value of the digital elevation model at the grid point corresponding to the k-th element of the mask, DEM_0 is the value of the digital elevation model at the grid point corresponding to the center element of the mask and MSlope is the defined maximum allowed slope. The result of this change in the algorithm is a shift in the resulting isolines. It should be noted that the methods to obtain the shortest path remain the same. These methods will be further covered below. The example below shows the results obtained by using the VTDT algorithm on the topography in figure 2.6.1. Note that the single object point used by the VTDT algorithm was at the center of figure 2.6.2.

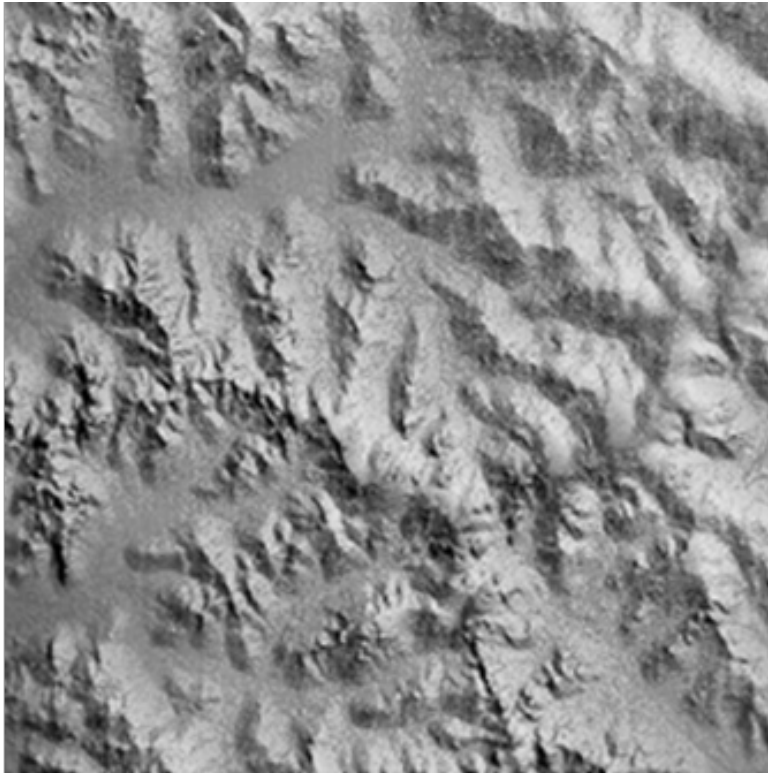


Figure 2.6.1: Example topography, digital elevation model of which is used for the variable topography algorithm resulting in the matrix visually depicted in figure 2.6.1. The scale is from black – lowest elevation in this topography- to white – highest elevation in this topography.

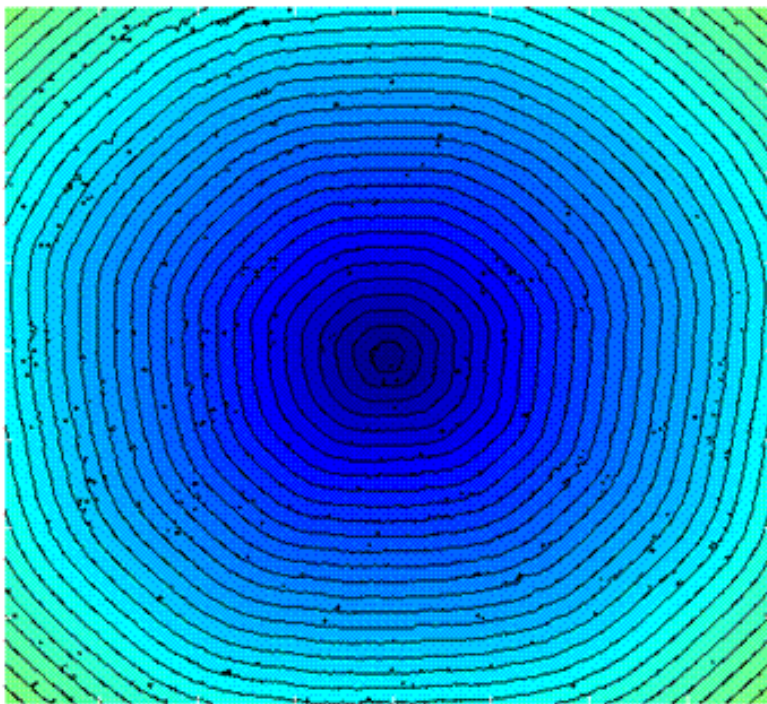


Figure 2.6.2: Visual representation of matrix resulting from using a variable topography distance transform algorithm on the a digital elevation model representing the topography shown in figure 2.6.1. The scale is from dark blue – lowest value of the resulting VTDT matrix - to green – highest value of the resulting VTDT matrix.

The use of VTDT has been proposed for geothermal pipelines in order to obtain the shortest route (Kristinsson, 2005), showing good results. The method employed in this study extends his method to include visual effects optimization along with the original objective of obtaining the shortest route (or in this case a sufficiently short route). The algorithm is modified to fulfill these goals as will be covered below. Another extension that will also be covered below is that a new distance transform based method of visual effects ranking is presented.

2.1.4 Multiple weight distance transforms

Multiple weight distance transforms (MWDT) were introduced by Smith (2004). A MWDT is an algorithm that utilizes multiple distance transforms, weighted based on relative importance, to obtain a minimum (or maximum). The simple version of the algorithm contains only one criterion (usually distance) but optimization with regard to multiple criteria is also possible. For the specific problem of obtaining optimal separator and power plant locations, criteria that are taken into account are distance, local incline and land availability. Resulting from a MWDT is a composite surface with one or more minima. It is utilized in this study with additional constraints to obtain the optimal location for separators and power plants. Following is the central function of the MWDT algorithm where $DT(A_i)$ represents the distance transform on set A_i , k_i the relative weight of set A_i and z the matrix resulting from the MWDT algorithm.

$$z = \sum_{i=1}^n k_i DT(A_i) \quad 2.4)$$

In figures 2.7.1 and 2.7.2 below is shown an example of how an unconstrained MWDT algorithm solves the problem that when given a set of points, to obtain the point with the least total distance to all the given points.

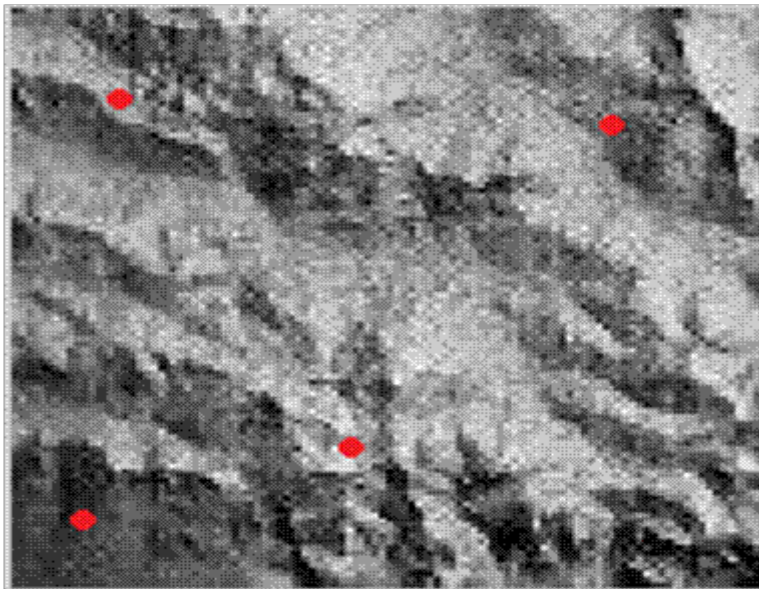


Figure 2.7.1: Example topography used for an unconstrained multiple weight distance transform algorithm example, the visual representation of the results of which is shown in figure 2.7.2. The red dots in the image represent the set of points for whom the point with the least total distance is obtained in figure 2.7.2. The scale is from black – lowest elevation in this topography- to white – highest elevation in this topography.

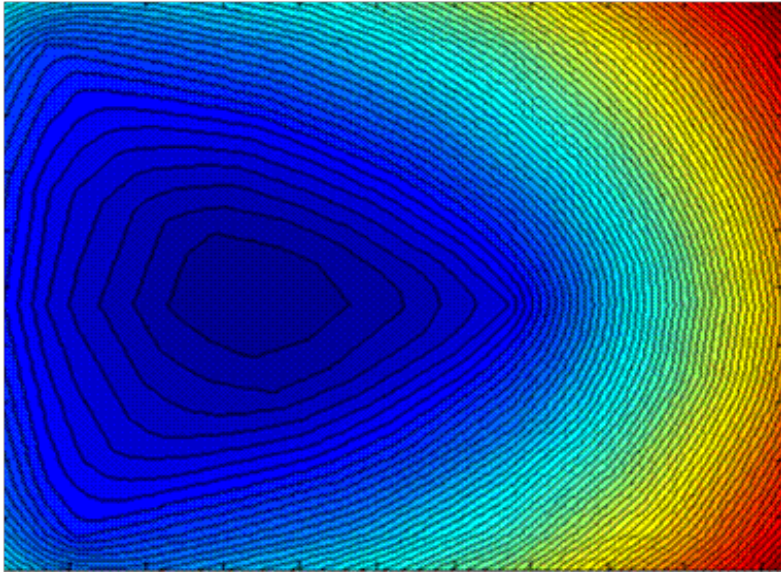


Figure 2.7.2: Visual representation of the results of using an unconstrained multiple weight distance transform algorithm on the example depicted in figure 2.7.1. The scale is from dark blue – points with the least total distance to the given set of points - to dark red – points with the highest total distance to the given set of points.

2.1.5 Non-accessible areas and distance transforms

Distance transform algorithms handle non-accessible areas by either modifying the digital elevation model used or introducing an extra pseudo objective function (when using a MLCDT – see chapter 3.2.2. For single-objective function DT's, pixels in the DEM corresponding to the non-accessible areas are given a very high value, this in effect means that when equations 2.2-3 are applied to a pixel in a mask, that incremental path is rejected, due to the maximum slope being exceeded. In figures 2.8.1 and 2.8.2 is shown the impact of including a non-accessible area in the application of the distance transform. In practice this can be anything from a lake to a residential area.

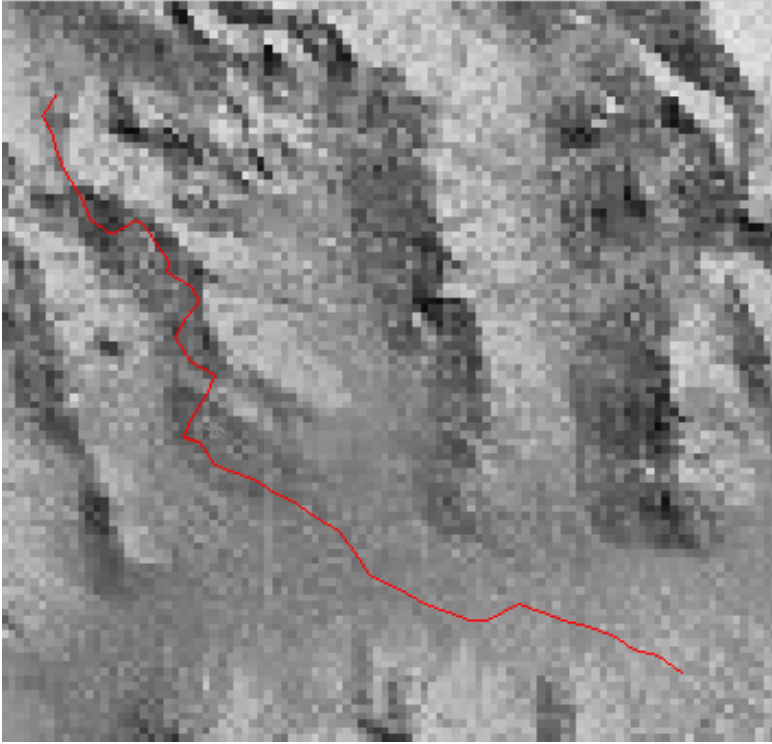


Figure 2.8.1: Variable topography optimal route without constraints on non-accessible areas. The optimal route is represented by the red line. The scale is from black – lowest elevation in this topography- to white – highest elevation in this topography.

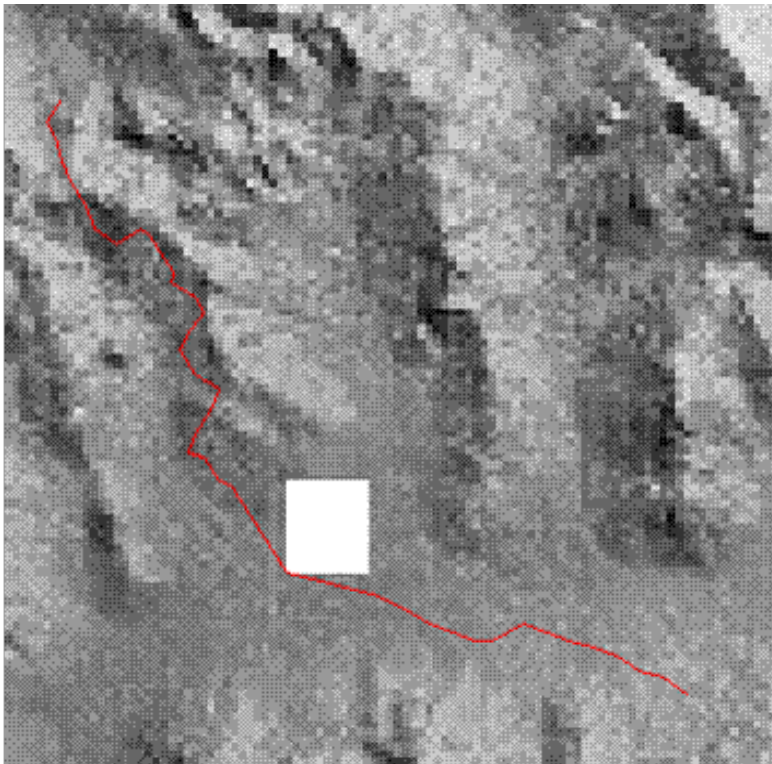


Figure 2.8.2: Variable topography optimal route with constraints on non-accessible areas. The optimal route is represented by the red line and the white area represents the non-accessible area. The scale is from black – lowest elevation in this topography- to white – highest elevation in this topography.

2.1.6 Optimal route with distance transform algorithms

To obtain the optimal route with distance transform algorithms two different approaches are possible. To consider first of all the simplest case, optimization with regards to a single objective – route length, the shortest path is known to be orthogonal to the distance isolines (distance bands) generated by the distance transform. After a start point is chosen, the first part of the shortest route is a line from that point orthogonal to the closest isoline, in the direction to the end point. The second part of the line is orthogonal to the next isoline. This process is then repeated until the end point is reached. The extension to multiple objectives – equal cost isolines – is straightforward. The same rules apply to equal cost surfaces (taking into account multiple objectives) as for equal distance isolines, the optimal route is similarly orthogonal to the equal cost isolines. The process is therefore the same.

A better solution is to record the incremental path movements as a part of the distance transform algorithm. The algorithm can be amended to record for each point in the grid, the direction to the next grid point, on the optimal path, to the start point. While this is essentially the same method as the previous one, this representation gives smoother and better results and requires less computation time. The upper limits on the accuracy of this method are the fineness of the grid in question, while the accuracy of the previous method is limited by the number of isolines generated. The accuracy of the second method is therefore greater, and indeed the upper limit on the accuracy of the first method, for a given grid, is the accuracy provided by the second method. The second method is also more computationally efficient, as the incremental path movements are simply recorded in a matrix of the same size as the original grid, simultaneously with the mask being placed on each grid point. The second method requires the computation of isolines after the distance transform matrix has been generated. The example depicted below in figure 2.9 shows typical isolines resulting from using a VTDT algorithm and the optimal path generated using the second method described above.

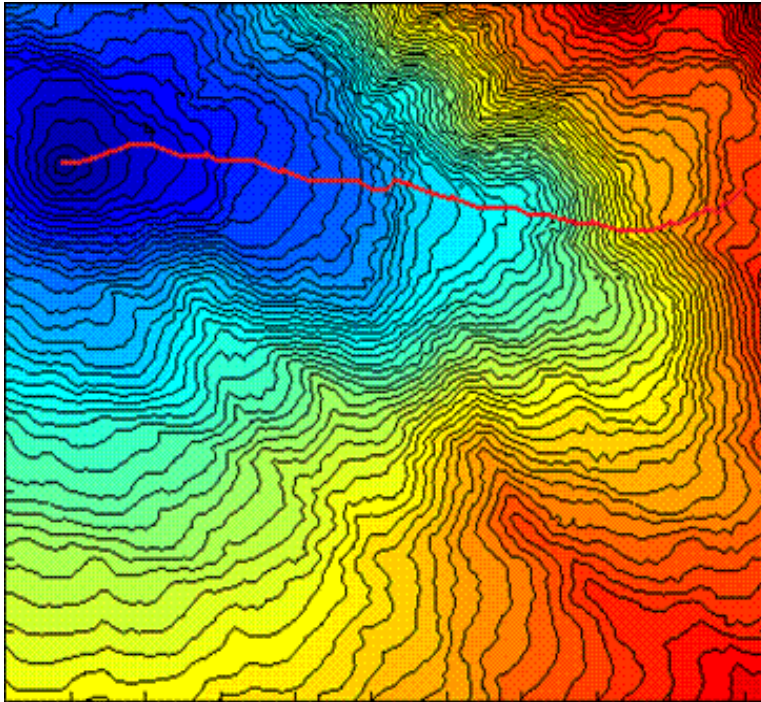


Figure 2.9: Example of an optimal path obtained with a variable topography distance transform algorithm using the method of recording incremental path movements to obtain the optimal route. The red line represents the optimal route and the scale is from dark blue – lowest value of the resulting VTDT matrix - to dark red – highest value of the resulting VTDT matrix.

2.2 Genetic algorithms

Genetic algorithms (GA) are optimization methods that use aspects of the natural evolution process (Arora, 2004). They are a part of the larger class of evolutionary algorithms. Genetic algorithm have been extensively used in engineering, computer science, bioinformatics, physics, manufacturing, economics and many other fields.

2.2.1 Basic principles

The basic idea of a genetic algorithm is that a population of individual solutions (chromosomes/strings) evolves in the direction of better solutions. A new set of solutions is produced from the solutions of the previous generation in a manner that the average fitness of the entire population of solutions improves. This evolution mirrors the natural evolution process. Genetic algorithms require only function values to further the process towards convergence, continuity and differentiability is not required or used in the algorithm. Due to this, genetic algorithms are very general and can be applied to a wide variety of problems – discrete, continuous and non-differentiable (Arora, 2004). The main drawbacks of genetic algorithms is first of all that they require a large number of function evaluations and secondly that they do not guarantee convergence to a global optima. The three classical operators in a genetic algorithm are selection, crossover and mutation, there are however many variations of GA's available with variations in those operators and additional operators.

Initialization

In most applications of genetic algorithms the initial population is randomly generated, this is however not always the case and it can be beneficial to have an initial population that represents more viable solutions than a randomly generated population would offer. This is especially the case when the solution space is exceedingly large (as is indeed the case for the problem of this study). To represent the design variable values in the strings, a few different encoding approaches are available. Binary encoding, where a variable is represented as a string of zeros and ones, is most common but real number encoding and integer encoding are also widely used. The size of the initial population is dependent on a number of factors such as the nature of the problem and the size of the search space.

Selection

For genetic algorithms, in the same way as for the natural evolution process, a selection process occurs. At each generation a number of individuals are selected, the next generation is then generated from those selected individuals through the use of the genetic operators, crossover and mutation, covered below. There are a multitude of different selection methods available for genetic algorithms; the common thread is that the methods are fitness-based. What this essentially means is that individuals with a higher fitness have a higher probability of selection. The fitness of an individual is determined through function evaluations. This can be for an example, the total length of a pipeline or the weight of an object.

The selection method used in this study is called tournament selection. A number of individuals (most commonly two or three) are selected from the entire population and these individuals compete for selection, mimicking the natural selection process. The fittest individuals (with the lowest or highest values, depending on the objective) are then selected for crossover. The selection method of this study and other methods used are further covered and detailed in chapter 3.3.

Crossover

The genetic operator corresponding to reproduction in the natural evolution process is called crossover. This is essentially the process of generating new children individual solutions from the parent individuals by combining or mixing the parent individuals. Most commonly two children are created from two parent individuals, however this can and does vary. There are a multitude of crossover methods available for genetic algorithms such as one point or two point crossover and uniform crossover. The selection method of this study is called a two point crossover. For two point crossover the two parent individuals are divided at two crossover points and from these parts the two children are created, essentially mirror individuals.

Mutation

Mutation is a genetic operator intended first of all to add additional diversity into the population and to prevent the loss of valuable genetic material in the selection and crossover steps (Arora, 2004). Mutation is a necessary step in the genetic algorithm that prevents convergence to local minima. Classically for a binary genetic algorithm the selection process would simply involve random selection of a number of individuals and randomly selecting a bit on the string and switching that bit from 0 to 1 or vice-versa. This can be much more complicated, especially for continuous and discrete genetic algorithms.

The mutation method of this study involves the random displacement of the discrete variables; this is covered further in chapter 3.3.

Termination

There are a number of methods for terminating a genetic algorithm, most commonly the GA will be terminated if certain criteria have been reached, for an example a sufficiently low cost of a mechanical part. Other methods include for an example termination having reached a certain number of generations, termination upon manual inspection or the allocation of a certain computational time to the algorithm. A combination of methods is also common. The algorithm of this study uses termination upon reaching a certain number of generations.

2.2.2 Multi-objective optimization and pareto genetic algorithms

For many optimization problems and specifically the problem of pipeline route optimization, there are multiple, often conflicting objectives. A multi-objective optimization problem (MOP) can be defined as obtaining a vector of design variables to minimize a vector of objective functions that often conflict with one another. Such a problem takes the form (Cheng & Li, September 1997):

$$\text{minimize } \{f_1(\vec{x}), f_2(\vec{x}), \dots, f_n(\vec{x})\} \text{ subject to } \{g_1(\vec{x}), g_2(\vec{x}), \dots, g_m(\vec{x})\} \leq 0 \quad 2.5)$$

Where $f_i(\vec{x})$ and $g_i(\vec{x})$ are the objective and constraint functions. For a maximization problem or a mixed-objective the objective function would be normalized and the form of problem would be the same as above.

The main problem with solving MOP's is that the multiple optimization objectives can be conflicting, even have completely opposing aims. For an example for the problem of pipeline optimization the first and most obvious performance estimate is the pipeline length. The optimal solution is obviously a straight line from the start point to the end point. However with regards to two other performance estimates, the visual effects and incline, a straight line can be poorly performing solution. If it is desired to minimize the visual effects, the optimal route will be one that changes direction often in order to hide the pipeline as much as possible and in order to keep the incline low enough to avoid undesirable flow regimes and pressure waves a straight line will usually not be possible. The simplest solution to a MOP is to create a single objective function by using a weighted average of the constituent objective functions of the problem. Each objective function is given a relative weight factor and the performance index is then a simple sum of weighted cost functions. For n different cost functions, where w_i represents the relative weight of cost function $f_i(\vec{x})$, the performance index (PI) is then:

$$PI = \sum_{i=1}^n w_i f_i(\vec{x}) \quad 2.6)$$

The problem with this method is to determine the weight coefficients. This requires a careful examination of the cost functions and the relative importance of the optimization goals and in the end a judgment decision, which is in its nature, arbitrary. This method is used for the extension of the distance transform method in this study to multiple objectives as will be presented in chapter 3.2.

Pareto Genetic Algorithms

In multi-objective optimization there is usually no single optimal solution that performs better with regards to all the objectives. There is however a set of solutions that are equally optimal that are called pareto-optimal or non-dominated solutions. A solution is pareto-optimal if a solution cannot be found that performs better with regard to all the objectives. A vector of solutions \vec{x}' , where $f_i(\vec{x})$ are the objective functions, is pareto optimal if and only if (Cheng & Li, 1997):

$$f_i(\vec{x}) \leq f_i(\vec{x}') \text{ for all } i \in (1:m) \quad 2.7)$$

$$f_i(\vec{x}) < f_i(\vec{x}') \text{ for at least one } i \in (1:m) \quad 2.8)$$

The aim of a pareto genetic algorithm is to obtain this set of solutions. The effectiveness of a pareto genetic algorithm is usually defined by the distribution of the solutions on the pareto front. Figure 2.10 below shows a typical pareto optimal set and the distribution of the individual solutions on the pareto front for a maximization problem with two objectives.

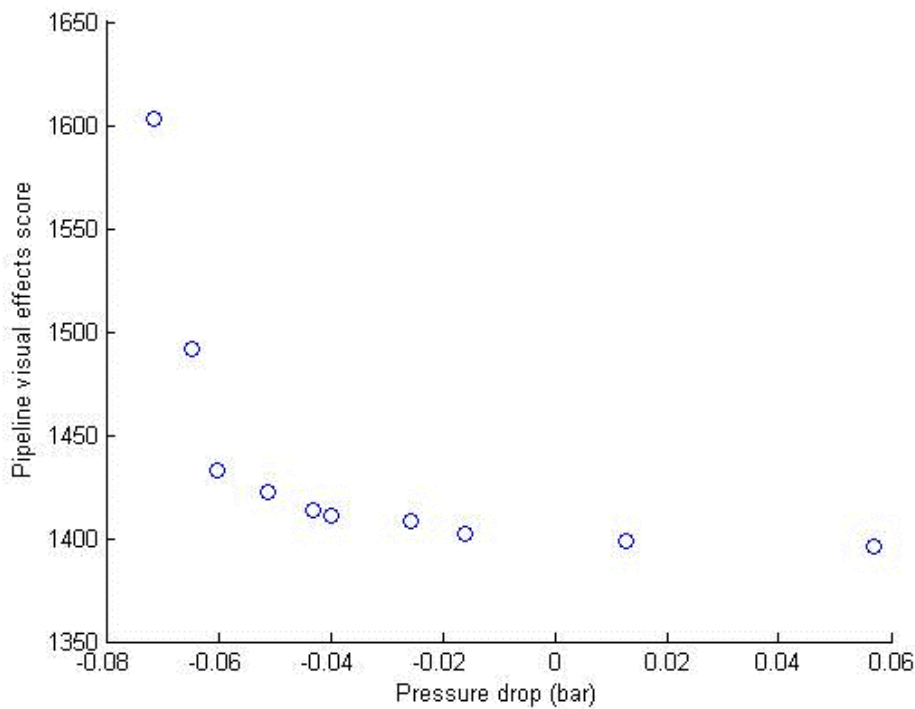


Figure 2:10: Example of a pareto optimal front obtained using the second method of this study on the Hverahlíð case study presented in chapter four. The two optimization objectives are pressure drop and pipeline visual effects score. The pareto optimal individuals are indicated by the blue circles in the figure. Note that this figure is the same as figure 4.12.

2.2.3 Non dominated sorting genetic algorithm

The Non-dominated sorting genetic algorithm (Srinivas & Deb, 1995) is based on the principle of non-dominated sorting (Goldberg, 1989) mentioned above. It was one of the first genetic algorithms created that use this principle but since its creation it has come

under some criticism (Deb, Agrawal, Pratap, & Meyarivan, 2002) leading to the creation of the Non-dominated sorting genetic algorithm II (NSGA II).

The basic idea of a NSGA is to use a non-domination ranking selection method to favor individual solutions that perform well and a niche method is then used in order to maintain stable subpopulations of well performing individuals (Srinivas & Deb, 1995). For the NSGA the crossover and mutation operators are unaltered, the only operator that changes from a conventional GA is the selection operator. As previously mentioned an individual/chromosome is non-dominated if no individual other individual in the population performs better with regards to all the objectives. The non-dominated individuals are given rank 1 (i.e they constitute the first front). They are then removed from the population. This process is then repeated with the rank progressively rising, until the entire population has been ranked. All individuals in each front are given a fitness value. The first front receives the highest value and with each front the fitness value progressively decreases.

In multi-objective optimization a genetic algorithm can have difficulties with maintaining diversity in the population. It has a tendency to converge to certain peaks and thus does not explore all the solution space. A genetic algorithm is based on the principles of biological evolution, where a variety of species exist. In genetic algorithms the corresponding phenomena is called a niche and it is desired to form multiple niches (i.e subpopulations) in order to maintain diversity in the population and prevent convergence to local minima. The population in genetic algorithms optimization is by necessity finite. This limited size along with the stochastic errors associated with a genetic algorithm cause the individuals of the population to become similar, in essence many individuals converging to a single optima. In order to combat this, a niching strategy is employed (Deb & Goldberg, 1989).

In the NSGA I a niching strategy called sharing is used. Sharing functions in a way that the fitness value of the individuals is effectively shared among the population. For each front a sharing function value between every pair of individuals is calculated.

$$C(d_{ij}) = \begin{cases} 1 - \left(\frac{d_{ij}}{\sigma_{share}}\right)^2, & \text{if } d_{ij} < \sigma_{share} \\ 0, & \text{otherwise} \end{cases} \quad 2.9)$$

Where $C(d_{ij})$ is the sharing function value for two individuals, d_{ij} represents the objective space distance between two individuals in the same front and σ_{share} the defined sharing parameter. For each individual its sharing values with all the other individuals are added together, this is called a niche count. An individual's fitness (the fitness value of all the individuals in the front) is then divided by the niche count. This results in a shared fitness value which is used for the selection process.

2.2.4 Non-dominated sorting genetic algorithm II

The NSGA II addressed 3 problems with the NSGA algorithm: First of all the overly high computational complexity of the non-dominated sorting, rendering optimizations with large populations very computationally intensive when using the NSGA (Deb, Agrawal, Pratap, & Meyarivan, 2002). Second of all the NSGA II addressed the lack of an elitist

strategy in the NSGA and thirdly it addressed the fact that the NSGA did not propose a value or a method to calculate the sharing parameter (see above).

Faster non-dominated sorting method

For the NSGA II algorithm the sorting method is different from the NSGA I, with the computational complexity being less (Deb, Agrawal, Pratap, & Meyarivan, 2002). For each chromosome i the number of chromosomes that dominate it n_i and the set of individuals that it dominates S_i is calculated. All the non-dominated individuals are gathered as the current front. For the sets S_i corresponding to the individuals in the current front, each time an individual appears in the set its count n_i drops by one. When the count n_i of a chromosome reaches zero it becomes part of the next front. The first front receives the rank 0 with the rank rising with each front. This process is repeated until all the chromosomes have been ranked.

Local crowding distance and crowded comparison operator

In addition to an individual's non-domination rank, in the NSGA II for each individual an attribute called local crowding distance is calculated. The local crowding distance of an individual has one component for each optimization objective and the value of each component is the average of the two adjacent objective function values. The crowding distance of the i -th individual is then the average side length of a cuboid enclosing the objective function values of the $(i-1)$ -th, i -th and $(i+1)$ -th individuals. To guide the selection process in the algorithm a crowded comparison operator is introduced which functions in the way that if two individuals have the same non-domination rank, the fitness of the individual with the higher crowded crowding distance value is in effect higher, i.e. that individual is preferred (Deb, Agrawal, Pratap, & Meyarivan, 2002).

Elitism

To introduce elitism into the algorithm the following procedure is incorporated into the selection method of the algorithm. The NSGA II forms a combined population, at each generation, of the parent and children populations. If the population size of the algorithm is N individuals the combined population will have $2N$ individuals. This population is then ranked according to non-domination. The parent population is created by adding to it the successive non-domination fronts until its size becomes larger than N . Then the crowded comparison operator is used to select points from the last non-domination front until the total parent population size reaches N . This is then the population used for selection, crossover and mutation. For the selection process binary tournament selection is used with the crowded comparison operator.

2.3 Pressure drop of two-phase flow in pipelines

Several different methods for calculating the pressure drop of two phase flow in pipelines have been proposed (Woldesemayat & Ghajar, 2007). Separated flow models are a class of commonly utilized models (Thome, 2006) for calculating the two phase drop, they employ two artificial pipes, one carrying the single phase gaseous phase and the other the liquid phase. The resulting two-phase pressure drop is then calculated from the single-phase pressure drops. Varying in many of the models is the correlation used for calculating the void fraction, which is essential to estimating the two phase pressure drop from the single

phase calculations. Pressure drop in two-phase flow in geothermal pipelines consists mainly of static pressure drop, momentum pressure drop and frictional pressure drop. Below are shown the methods used in this study to calculate the respective pressure drop components.

In this study the pseudo flow model of Harrison (1975) and Zhao, Lee & Freeston (2000) is used for pressure drop calculations. The Harrison-Zhao model has been shown to be effective (Zhao, Lee, & Freeston, 2000) in predicting the pressure drop in two phase pipelines. This method relates the pressure drop of a two phase system to that of pseudo-single-phase system which has the same pressure drop. It assumes that the pseudo single-phase flow has the same boundary layer velocity distribution as the two phase flow (Zhao, Lee, & Freeston, 2000). The average velocity of the pseudo flow is used to determine the qualities of the flow and the two phase pressure drop using conventional methods for a one phase system.

The total pressure drop is calculated with the following equation, where pressure drop in bends is taken as a special component of the total pressure drop. This is due to it being calculated in this study by special methods, it should be noted however that pressure drop in bends is a combination of the three main pressure drop factors in equation 2.10.

$$\Delta P_{\text{total}} = \Delta P_{\text{static}} + \Delta P_{\text{momentum}} + \Delta P_{\text{frictional}} + \Delta P_{\text{bends}} \quad 2.10)$$

Two parameters that will be used extensively in the pressure drop calculations are mass velocity and the void fraction. In the equation below \dot{m}_v represents the mass velocity, \dot{m} the mass flow rate and A is the pipeline cross sectional area.

$$\dot{m}_v = \frac{\dot{m}}{A} \quad 2.11)$$

Cross sectional void fraction:

$$\epsilon = \frac{A_g}{A} \quad 2.12)$$

Where A_g is the area of the gas phase, A the total area and ϵ represents the void fraction.

Static pressure drop

The static pressure drop is the pressure drop due to the elevation head (the gravitational pressure drop). For a two phase flow it is calculated using the homogeneous density which is the density averaged for the two flows using the void fraction.

Homogeneous density:

$$\rho_H = \rho_g \epsilon + \rho_l (1 - \epsilon) \quad 2.13)$$

Where ρ_g and ρ_l represent the densities of the gas and liquid phases. The static pressure drop is then calculated using the following equation:

$$\Delta P_{\text{static}} = \rho_H g \Delta H \quad 2.14)$$

Frictional and momentum pressure drop

The momentum pressure drop in the pipe is the pressure drop component due to the kinetic energy change in the flow. The momentum pressure drop between two points in a pipe is calculated from variation in the properties of the flow at the points. For an evaporating flow the kinetic energy of the flow increases as more of the fluid evaporates. This is due to the density of the vapor phase being less than that of the liquid phase and it results in a momentum pressure drop. If the flow is condensing the situation is reversed and the pressure increases. Equation 2.15 below is used to calculate the momentum pressure drop. However as equation 2.21 shows the momentum pressure drop can be included in the calculations for the friction pressure drop using the method of Harrison and Zhao.

Momentum pressure drop:

$$\Delta P_{\text{momentum}} = \dot{m}_v^2 \left(\left[\frac{(1-x)^2}{\rho_l(1-\epsilon)} + \frac{x^2}{\rho_g \epsilon} \right]_{\text{out}} - \left[\frac{(1-x)^2}{\rho_l(1-\epsilon)} + \frac{x^2}{\rho_g \epsilon} \right]_{\text{in}} \right) \quad 2.15$$

where x represents the steam quality. In the method of Harrison and Zhao, to predict the two-phase pressure drop, an equivalent pseudo single-phase flow is assumed. This artificial flow has the same boundary layer velocity distribution as the two-phase flow and it is the average velocity of this flow that is used to determine the friction coefficient of the flow (Zhao, Lee, & Freeston, 2000). As is shown below in equation 2.21 the pressure drop is then calculated using the friction coefficient. This has been shown to be in good agreement with experimental data (Zhao, Lee, & Freeston, 2000). The average liquid phase velocity and the wall friction factor were first used by Harrison (1975) to predict two-phase pressure drop, using the techniques developed for single-phase flows but Zhao, Lee, & Freeston (2000) extended the idea to the pseudo flow being that flow which has the same boundary layer velocity distribution as the two-phase liquid layer. In that article the correction factor $1.1(1-x)$ was also introduced into equation 2.16.

Liquid phase velocity:

$$\bar{V}_f = 1.1(1-x) \frac{\dot{m}_v(1-x)}{\rho_l(1-\epsilon)} \quad 2.16$$

Average velocity of equivalent single phase flow:

$$\bar{V} = \bar{V}_f \frac{(1-\epsilon)}{(1-\epsilon)^{8/7} (1 + \frac{8}{7} \sqrt{\epsilon})} \quad 2.17$$

The following equation for the void fraction that is utilized in this study was introduced by Zhao (2000):

$$\frac{1-\epsilon}{\epsilon} = \left(\left(\frac{1}{x} - 1 \right) \left(\frac{\rho_g}{\rho_l} \right) \left(\frac{\mu_l}{\mu_g} \right) \right)^{7/8} \quad 2.18$$

Two phase dynamic viscosity:

$$\mu_{\text{tp}} = x\mu_g + (1-x)\mu_l \quad 2.19$$

Where μ_g and μ_l are the viscosities of the gas and liquid phases respectively. The Reynolds number is calculated using the following equation:

$$Re = \frac{\dot{m}_v d_i}{\mu_{tp}} \quad (2.20)$$

Where d_i represents the inner diameter of the pipeline. The two phase friction factor is estimated by the following equation:

$$f_{tp} = \frac{0.316}{Re^{0.25}} \quad (2.21)$$

Combined frictional and momentum pressure drop:

$$\Delta P_{\text{friction+momentum}} = \frac{f_{tp} \bar{V}^2 L}{2d_i(1-AC)} \quad (2.22)$$

Where the acceleration correction factor is estimated by:

$$AC = \frac{\dot{m}_g}{\rho_g p A^2 \epsilon} \quad (2.23)$$

Where p is the pressure in the pipeline and \dot{m}_g represents the mass flow rate of the gas phase.

Pressure drop in bends

Pressure drop in bends for two-phase flow is calculated using the classical two phase multiplier method. In this study the Chisholm B-type multiplier, is utilized (Chisholm, 1979). As is shown in equation 2.28 the general pressure drop equation for other installations is similar to equation 2.26 for the pressure drop in bends. Equation 2.28 includes expansion loops, bends, valves and connections and the two phase multiplier from equation 2.23 is the same, what differs is equation 2.24 for the constant K .

Two-phase multiplier for bends (Chisholm, 1979):

$$\varphi_b^2 = \left(\frac{1}{(1-x)^2} \right) \times \left(1 + \left(\frac{\rho_l}{\rho_g} - 1 \right) (Kx(1-x) + x^2) \right) \quad (2.24)$$

Where:

$$K = 1 + \frac{2.2}{1.6f h_b \left(2 + \frac{r}{d_i} \right)} \quad (2.25)$$

Where r represents the bend radius, f the friction coefficient and h_b is the equivalent length. The bend pressure drop is then:

$$\Delta P_{\text{bends}} = \frac{dP}{dz} \Big|_{lb} \varphi_b^2 n_b h_b d_i \quad (2.26)$$

Single phase flow pressure drop:

$$\left. \frac{dP}{dz} \right|_b = \frac{f \rho_h \bar{V}^2}{2d_i} \quad (2.27)$$

The general pressure drop equation for bends, expansion loops, valves and connections is:

$$\left. \frac{dP}{dz} \right|_l = \frac{f \rho_m \bar{V}^2}{2d_i} (\varphi_b^2 n_b h_b d_i + \varphi_{eu}^2 n_{eu} h_{eu} d_i + \varphi_c^2 n_c h_c d_i + \varphi_v^2 n_v h_v d_i) \quad (2.28)$$

Where n_b , n_{eu} , n_c and n_v represent the number of bends, expansion units, connections and valves respectively. The equal length symbols are: h_b , h_{eu} , h_c and h_v . The two phase multipliers for expansion units, connections and valves (φ_{eu}^2 , φ_c^2 and φ_v^2) are similar to the two phase multipliers for bends.

3 Adjustment of methods for route optimization

This chapter presents all the adjustments and additions, to the methods of chapter 2, of this study. It should be clearly noted that all of the innovations of this study are contained in this chapter. In the first part of this chapter a new method of ranking points in a given topography based on visual effects is presented. In the second and third parts are covered the adjustments and innovations relating to the distance transform based method and the genetic algorithm based method respectively.

3.1 Distance transform visual effects ranking

As previously stated the main goal of this study is to design an effective methodology to optimize the pipeline route with regards to visual effects. In order for this to be possible, a logical first step is to obtain some sort visual effects ranking of the different locations in a geothermal area. In essence it is necessary, before any optimal path algorithm is used on a DEM of a geothermal area, to rank all the pixels with regards to the visual effects that a pipeline in that location would cause. Distance transforms with their ability to register the shortest path from all points to the central point used in the transform present a way to achieve this.

When a simple unconstrained distance transform is performed with only one object point, the shortest path from all points to this object points will be a direct line. That is, the shortest path registered by an unconstrained simple DT algorithm is the line of sight. Since the DT algorithm can be amended to register all the points between the object point and a selected point, the next step is for the algorithm to obtain information about the properties of all the points between the selected point and the object point.

The proposed method of this study is to calculate a DT for every point in the image, from each point to multiple selected points, for whom it is desired to minimize the visibility of the pipeline (roads, towns, tourist sites, etc). Between each pixel and all the selected observation points, the DT algorithm records all the points between the respective points. For each pixel the height of all the points between the pixel (object point) and the observation points is recorded. The height of the line of sight is then calculated and then the algorithm calculates if at any point the line of sight from observation point to the object point is interrupted. If it is interrupted, that is if the object point is not visible from the observation point, the pixel gets a full score with regards to this observation point.

When observing a pipeline from afar, it is clearly most visible when the line of sight is not interrupted and when the area behind the pipeline in the line of sight is clear, that is if the surface behind the pipeline is lower than the line of sight. The observer sees the pipeline much more clearly if only the horizon or some geography a substantial distance away from the pipeline is viewed behind it. Indeed in the Icelandic geothermal industry today, engineers responsible for route design attempt to first of all hide the pipeline as previously explained, and second of all if this is not deemed practical, to make sure that behind the pipeline (in terms of the line of sight) is an obstacle (close by) that interrupts the line of sight. It should be noted that this effort is manual and not optimized in any way. For this

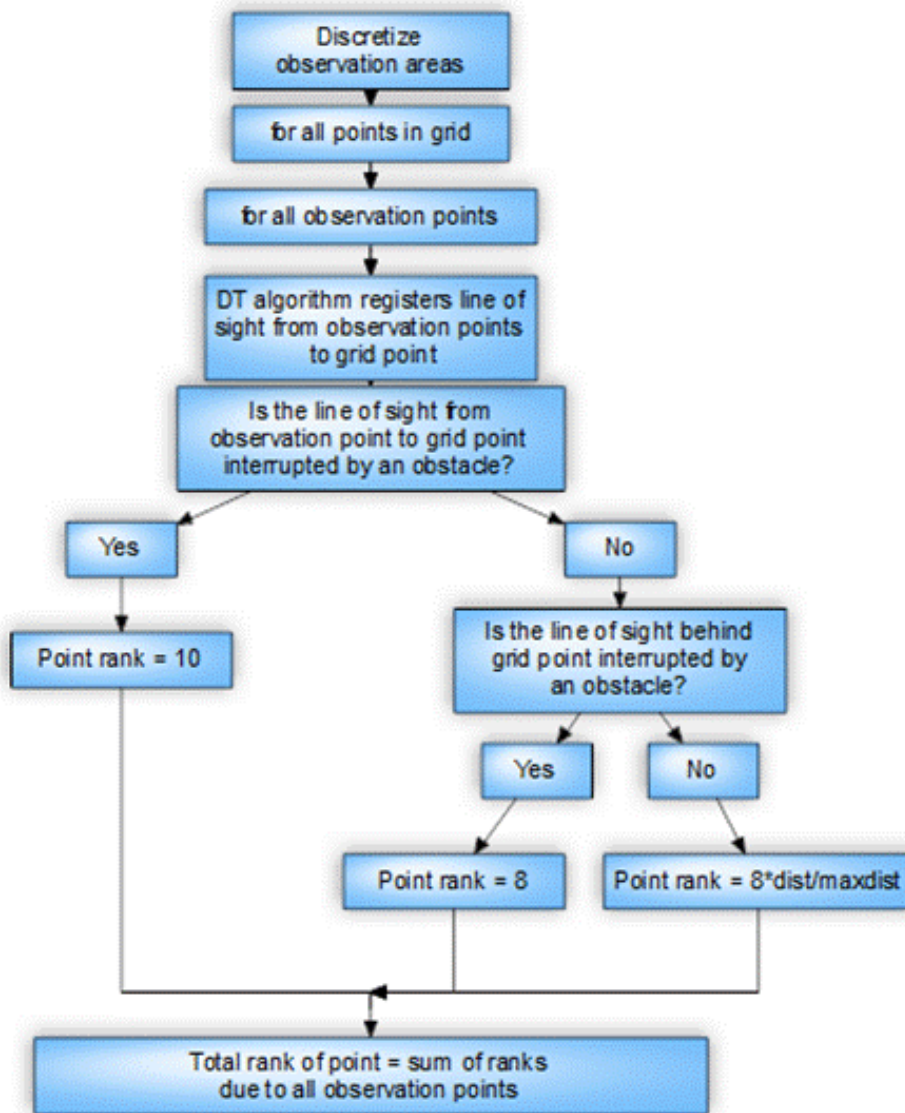
ranking method, this is incorporated. If the line of sight is not interrupted, on either side of the point in question, the score of that point is proportional to the distance to the observation point. If it is farther away, the visibility declines and the score will be higher. The total score of each pixel is the sum of the score for this pixel due to each observation point. Algorithms 1-1 and 1-2 below display the algorithm of the visual effects ranking method.

```

for j = 1 to ydim
  for i = 1 to xdim
    get DEM(i,j)
    for k = 1 to NumObs
      [r,s] = ObsPoint(k)
      get DEM(r,s)
      run a simple distance transform between [r,s] and [i,j]
      Dist = result of distance transform
      Route = incremental path movements from [r,s] to [i,j]
      SightRoute = calculated line of sight from [r,s] to [i,j]
      if any Route(l) ≥ SightRoute(l), l = [1: size(Route)]
        rank(k) = 10/Numobs
      elseif any(SightRoute((i + 1):(i + tol), (j + 1):(j + tol)) ≥ DEM(i,j))
        rank(k) = 8/Numobs
      else
        rank(k) = 8 *  $\frac{Dist}{MaxDist}$ 
      end
      TotalRank(i,j) = sum(rank)
    end
  end
end

```

Algorithm 1.1: Distance transform visual effects ranking



Algorithm 1.2: Distance transform visual effects ranking – visual representation

Below is an example of how the algorithm functions. It is used on the sample area in figure 3.1.1 where the red line represents the observation line (f.a.e a road) that is discretized into the observation points used in the algorithm. The results from the visual effects ranking used on the example in figure 3.1.1 are shown in figure 3.1.2.

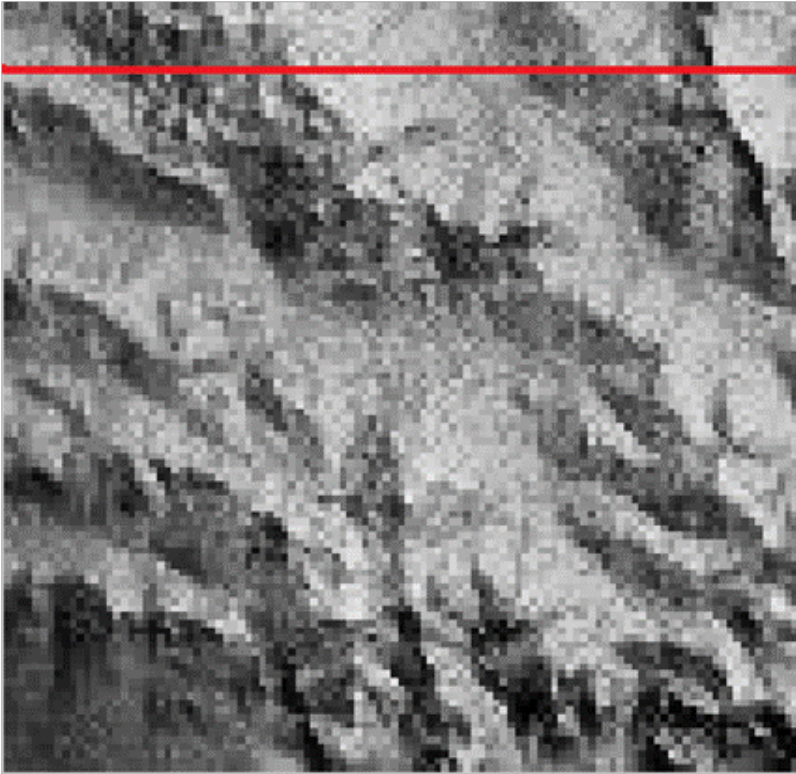


Figure 3.1.1: Example topography and road used for visual effects ranking algorithm example, the results of which are depicted in figure 3.1.2. The red line represents the road that is defined as an observation area and discretized. The scale is from black – lowest elevation in this topography- to white – highest elevation in this topography.

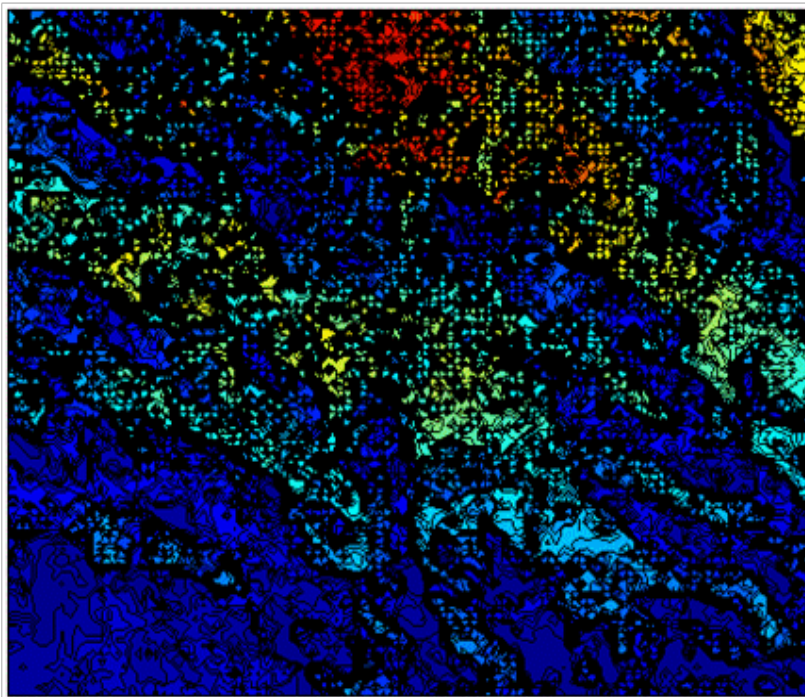


Figure 3.1.2: Visual representation of matrix resulting from using the visual effects ranking algorithm on the example depicted in figure 3.1.1. The scale is from dark blue – lowest visual effects score – to dark red – highest visual effects score.

3.2 Distance transform based method

3.2.1 Constrained multiple weight distance transforms

The problem of obtaining the optimal location for separators is essentially: for a given set of points, to find the point with the least total distance to all the given points. A geothermal area in utilization will have a number of boreholes and it is desirable to be able to select a separator location with the least total distance to the borehole, or a gathering point for a pipeline to carry the brine from all the boreholes to a separator located closer to the power plant. Alternatively it might also be desired to select the location of the power plant in a similar way. A multiple weight distance transform algorithm can solve this problem as was covered in chapter 2.1.4.

In geothermal areas, and in other areas where the same location selection procedure might be used, there are many areas that are inaccessible and therefore unavailable to be used as separator/power plant locations. For an example this might be lakes or rivers. There are also areas where it is not desirable to place a construction, such as very close to habited areas or a wildlife reserve. Another important factor in the selection of locations for construction is the incline at the site. It is not practical to choose locations where the incline is very steep. Therefore it is desired to include in the method a way to exclude these areas from selection. In this study this is done by the introduction of an extension to the multiple weight distance transforms called constrained multiple weight distance transforms (CMWDT) and by the inclusion of an additional matrix for the inaccessible areas. The extension of MWDT's to include constraints is simple and mirrors the extension of regular distance transforms to include incline constraints. For every one of the component DT's in the MWDT there are included incline constraints in the same way as shown in equations 2.2 and 2.3, the only difference is that the incline constraints must be in both directions, away from and to the distance transform starting point. To include non-accessible areas a matrix is created with very high values for inaccessible areas and zero for accessible areas, this matrix is then added to the component matrices of the CMWDT. An example of a CMWDT is shown below in figures 3.2.1 and 3.2.2

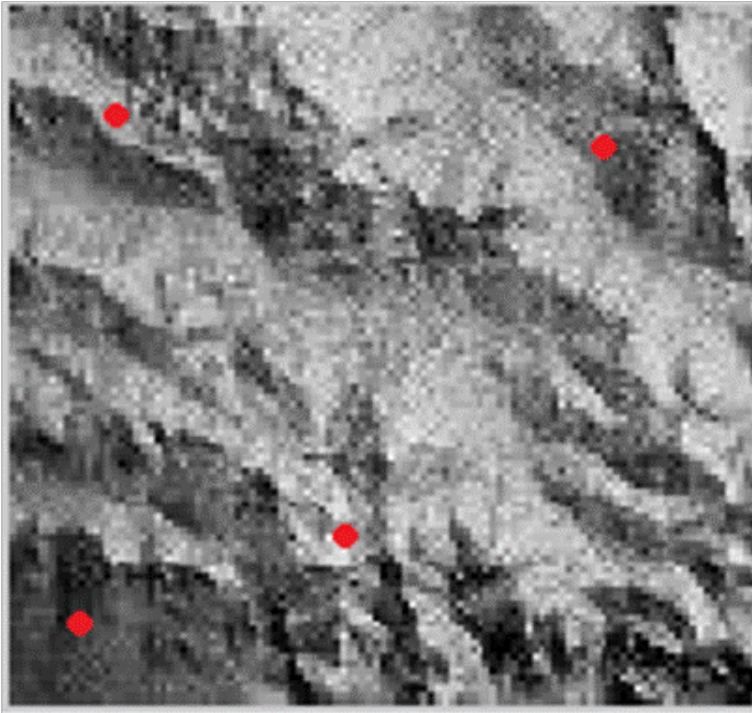


Figure 3.2.1: Example topography used for a constrained multiple weight distance transform algorithm example, the visual representation of the results of which is shown in figure 3.2.2. The red dots in the image represent the set of points for whom the point with the least total distance is obtained in figure 3.2.2. The scale is from black – lowest elevation in this topography- to white – highest elevation in this topography.

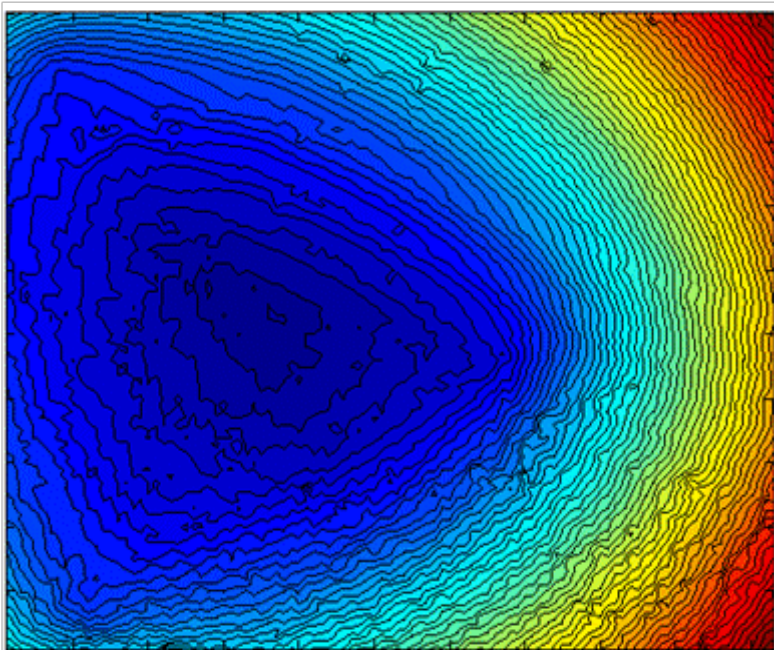


Figure 3.2.2 Visual representation of the results of using a constrained multiple weight distance transform algorithm on the example depicted in figure 3.2.1. The scale is from dark blue – points with the least total distance to the given set of points - to dark red – points with the highest total distance to the given set of points.

3.2.2 Multi-objective least cost distance transforms

It is possible to modify the distance transform algorithm to incorporate cost functions (for an example in this case land costs and visual effects). This was first presented by Smith (2004) as the least cost distance transform algorithm (LCDT) and is extended here to incorporate multiple cost variables. It should be noted that the extension of the LCDT to include multiple cost function was suggested by Smith (2004) and therefore the contribution of this study to the LCDT is the implementation of that suggestion. The costs of each variable need to be defined in each pixel and these costs are then multiplied to the incremental distance to each lattice point. The central function of a MLCDT with n cost variables is:

$$d_0 = \min(d_k + \text{LDM}(k) * (\text{cost}_1(x, y) + \text{cost}_2(x, y) + \dots + \text{cost}_n(x, y)), d_0) \quad 3.1)$$

The extension to the VTDT is:

$$\text{slope} = \frac{\text{DEM}_k - \text{DEM}_0}{\text{LDM}(k)} \quad 3.2)$$

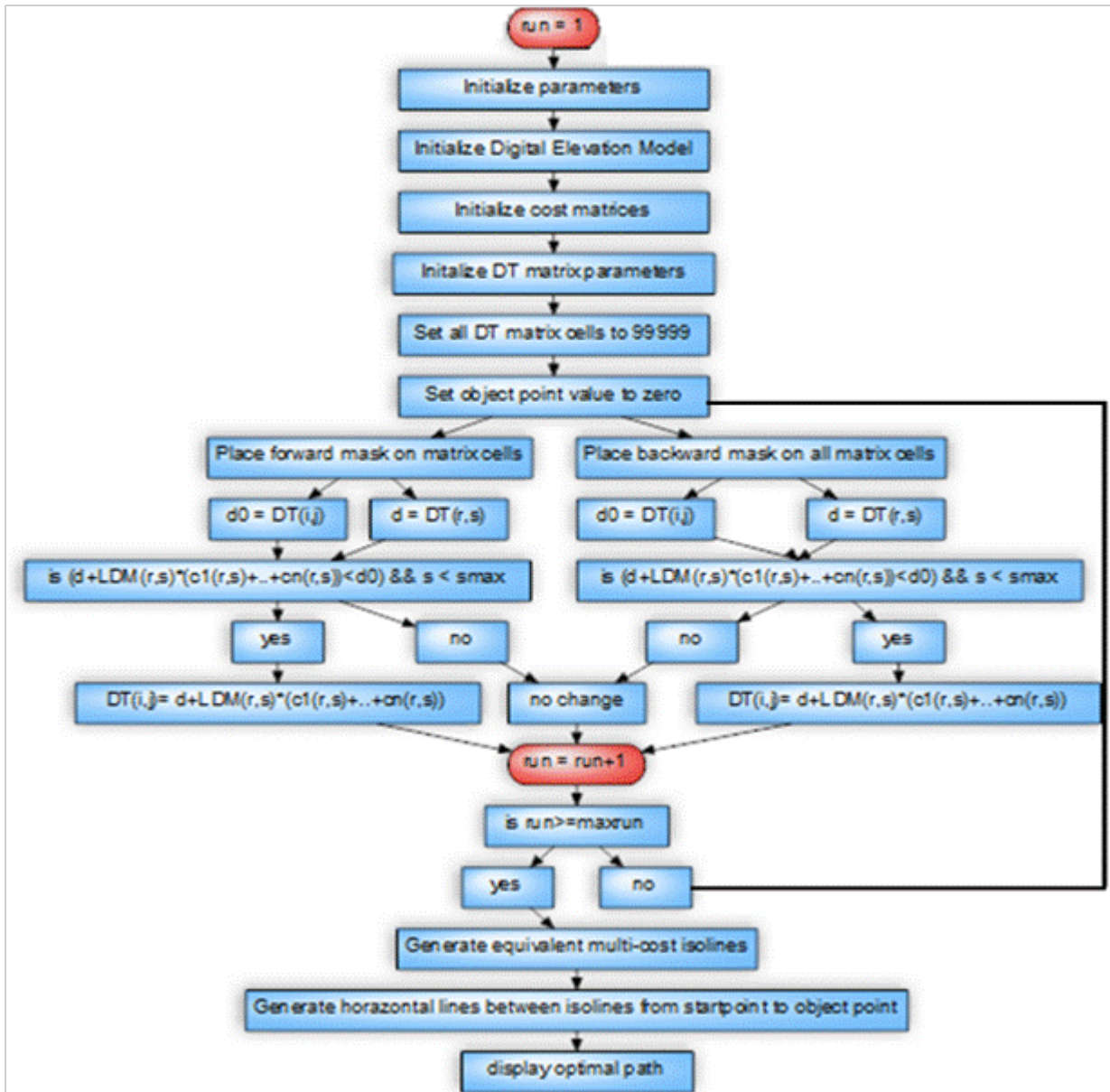
$$\text{if} (d_k + \text{LDM}(k) * (\text{cost}_1(x, y) + \dots + \text{cost}_n(x, y)) < d_0 \ \&\& \ \text{slope} < \text{MSlope});$$

$$\text{then: } d_0 = d_k + \text{LDM}(k) \quad 3.3)$$

Where d_k is the grid point value of the k -th element in a chamfer mask, $\text{LDM}(k)$ is the local distance metric, d_0 the current value of the grid point at the center of the chamfer mask. DEM_k represents the height of the digital elevation model at the grid point corresponding to the k -th element of the mask, DEM_0 is the height of the digital elevation model at the grid point corresponding to the center element of the mask, $\text{cost}_n(x, y)$ represents the n -th cost function and MSlope is the defined maximum allowed slope. The isolines generated by this algorithm are then equal cost isolines and the surface created is an accumulated cost surface.

As mentioned in chapter 2.1.5 the MLCDT extension to DT's offers the possibility of another approach to including inaccessible areas in the DT optimization. Instead of changing the value of the DEM in pixels corresponding to non-accessible areas, a pseudo cost function matrix can be created that represents non-accessible areas. The non-accessible areas cost function matrix will have very high values for all the non-accessible areas. The ratio of the non-accessible area pixel value to the sum of the maximum values of all other cost functions multiplied by the maximum local distance metric value is set at a high value (say 99999), in order to guarantee that non-accessible areas will not be chosen by the MLCDT. All grid points in the matrix corresponding to accessible areas will have the value 1.

It is necessary when employing a MLCDT algorithm to pay heed to the relative weight and size of the different cost functions. It is in essence up the designer to normalize the cost functions and choose the relative weight coefficients. This is a known problem in multi-objective optimization and one that is often without straightforward answers. This is a disadvantage of this method but it should not be too great. The method should still be an effective aid to the design process, even if some trial and error will be necessary.



Algorithm 2: Multi-objective least cost distance transform

3.2.3 GA modification of DT route

The problem of modifying the route provided by the DT method with regards to expansion loops is a problem that a genetic algorithm can handle well. The objective is to modify the route to include necessary expansion loops in order to account for the thermal expansion of the pipeline. The primary objective of the GA modification is to obtain the optimal placing for the expansion loop with regards to visual effects. Another objective of the modification is to regulate the frequency of bends in the route. Depending on the resolution of the DEM the DT route can vary considerably and for practical reasons it is not desirable for the pipeline to include bends at too frequent intervals. The first step in the route modification is to discretize the DT route. The input route into the GA is the route directly through the discretized points. The discretization resolution is an input into the algorithm. An example of this is shown in figure 3.3 below:

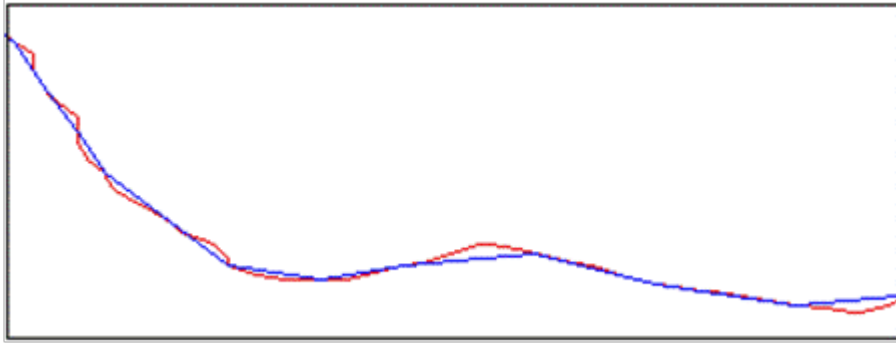


Figure 3.3: Example of discretization of a pipeline route. The red line represents the original distance transform provided route that is discretized and whose number of bends is regulated. The blue line represents the route resulting from the genetic algorithm modification of the red distance transform provided route.

The inputs into the GA algorithm are the route resulting from the discretization of the DT route, the number of expansion loops, maximum distance between expansion loops, size of expansion loops (the algorithm can also include the size of expansion loops as a variable with constraints on maximum and minimum size) and the discretization resolution. The GA is standard, employing binary tournament selection, two point crossover and mutation, with constraints on the expansion loop relative locations. For every expansion loop, its location on the route and on which side of the route it is placed are variables in the GA. A constraint included in the GA is incline at the site of the expansion loop, which needs to be limited for obvious practical reasons. Therefore the GA used the DEM of the area to implement the incline constraint by way of a simple penalty function. Below in figures 3.4.1 and 3.4.2 is an example of a VTDT route obtained for the Hverahlid geothermal area in Iceland and the subsequent GA modification of that route.

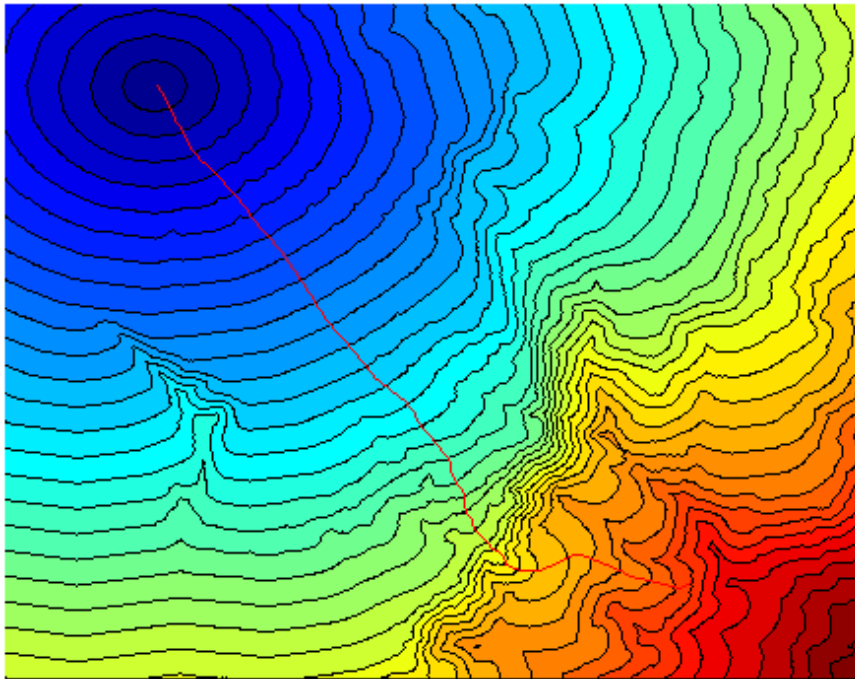


Figure 3.4.1: Visual effects isolines and optimal route obtained using the distance transform based method. The red line represents the optimal route and the scale is from dark blue – lowest value of the resulting VTDT matrix - to dark red – highest value of the resulting VTDT matrix.

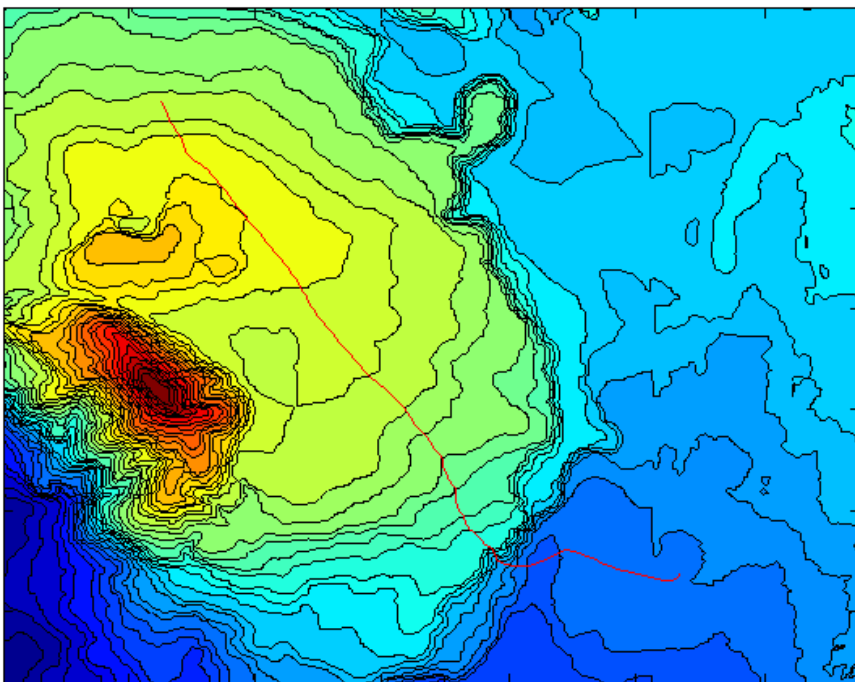
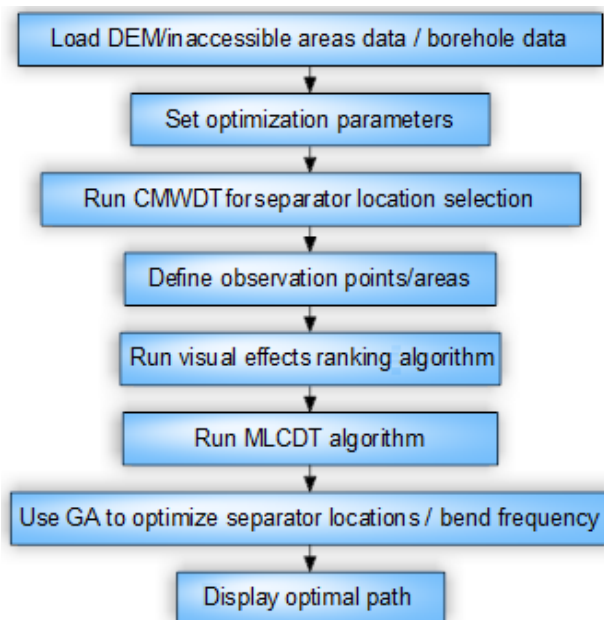


Figure 3.4.2: Digital elevation model of Hverahlíð geothermal area and optimal route obtained using the distance transform based method. The red line represents the optimal route and the scale is from dark blue – lowest altitude – to dark red – highest altitude.

3.2.4 Summary of distance transform based method

The first step in the method is to load the digital elevation model of the geothermal area in question, and data about inaccessible areas – note that further work can be required with this data for it to be in the matrix form necessary to function with the MLCDT. Also data about borehole locations (and separator /power plant locations depending on available data) is required. The next step is to define the optimization parameters, which mainly means defining the maximum incline in both directions, and the maximum distance for the visual effects ranking. The borehole data is then used for the CMWDT algorithm to determine the optimal separator / gathering point locations. In the fourth and fifth steps the observation points/areas are defined and discretized and algorithm 1 – the visual effects ranking algorithm - is run. The next step is to run algorithm 2 - the MLCDT algorithm and subsequently the simple GA is utilized to optimize the expansion unit locations. Finally the optimal route is displayed.



Algorithm 3: Distance transform based method

3.3 Genetic algorithm based method

3.3.1 Motivation

As will be discussed further in the case study of chapter four, the DT based method performs well in optimizing only with regards to the visual effects and it also offers the possibility of including multiple cost functions. There are however some limitations to the DT based method. First of all, if any objective is to be included in the optimization, it is required that it be represented in the form of a matrix where every grid point has the value of the cost function in the topographical location corresponding to that grid point. This is not always possible, f.a.e this makes it impossible to include the pipeline pressure drop as an objective. The pressure drop in geothermal pipelines is often significant and therefore it would be beneficial to the design process to be able to optimize both with regards to the visual effects of the pipeline and the pressure drop in the pipeline. It would especially be

beneficial to the design process to be able to choose from multiple options with regards to these objectives. Secondly in order to estimate the effectiveness of the DT based method it would be beneficial to compare the resulting route obtained using that method to routes obtained using a method known to be effective. Therefore the NSGA II is chosen as the basis for the second method of this study (Deb, Agrawal, Pratap, & Meiyarivan, 2002).

3.3.2 Genetic algorithm population generation using visual effects ranking and inaccessible areas

Creating an initial population when using genetic algorithms for pipeline routing can represent a problem. The area in question can be a several square kilometers in size and with digital elevation models readily available with a resolution as low as $(25 \times 25) \text{cm}^2$ the possible pipeline routes are of a number too large for a normal genetic algorithm to be a practical method of solution. Therefore this study presents a method that constrains the individuals created within an area deemed to be reasonable. An individual will consist of M variables representing points the pipeline route passes through. The initial values of the variables in an individual are selected by using binary tournament selection within the constrained area.

First of all an unconstrained distance transform algorithm is run from the start point of the pipeline (separator / gathering point) to the end point of the pipeline (power plant / separator). The route the DT algorithm registers, which for an unconstrained DT algorithm is a direct line, is used to discretize the x and y distance from the start point to the end point with the number of discretized points being equal to the number of variables M . Then for each individual a constrained area is formed for the M variables in the individual. For each discretized point in a given individual, a tolerance in both directions perpendicular to the direct line is defined and the square formed by the respective tolerances represents the constrained area for the initial value of its variables.

The next step is choose the initial value for each variable in an individual, i.e where in the tolerance area each point in a pipeline individual is placed. The obvious choice here is to select at random. However since the optimization will include two main optimization objectives, visual effects and route length minimization, it is logical to also constrain the initial individuals to perform well with regards to visual effects. Therefore the method uses binary tournament selection for each variable in every individual to choose its initial value. For each variable binary tournament selection is performed, where the tolerance area for each variable represents the tournament selection population. In the binary tournament selection the point with lower visual effects ranking value is selected. In the example shown in Figure 3.5, the visual effects ranking matrix used to generate the initial individuals and three of the pipeline routes generated are shown.

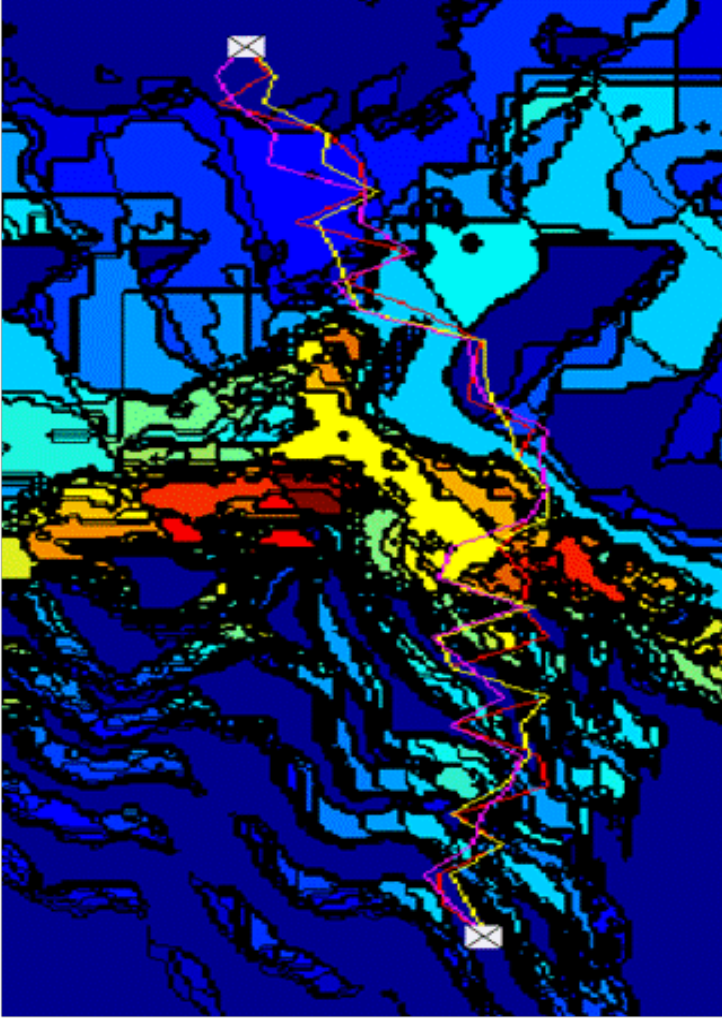


Figure 3.5: Visual effects ranking matrix and initial pipeline routes (individuals) generated using the initial population generation algorithm. The scale is from dark blue – low visual effects ranking – to dark red – high visual effects ranking. The purple, yellow and red lines are the generated routes.

3.3.3 Individuals and genetic operators

The individuals in the GA optimization are made up of discrete GA variables, as seen above in how the initial individuals are generated, with the number of variables depending on the decided resolution. Some of the main decision points when utilizing genetic algorithms involve choosing between the many different variants available of the main genetic operators and then adapting those operators to the problem at hand.

Two point crossover was chosen for use in this study by a method of trial and error. Many different kinds of crossover methods were tried during the route optimization for the Hverahlíð geothermal area where two point crossover was deemed perform best for this specific problem. The two crossover points are randomly chosen within defined parts of an individual. At both ends of an individual there are defined tolerances where the crossover points cannot be placed, also there is defined a minimum distance between the two crossover points. The crossover frequency of 0.9 was also chosen by a method of trial and error.

The mutation operator presents a challenge when optimizing pipeline routes with GA's. Essentially the problem is not only to define the mutation frequency but also the method of mutation – the variation of the discrete variable positioning upon mutation. In the solution method of this study not only the mutation position is random, but also the direction and size of mutation of the variable randomly chosen for mutation. What this means, for a given variable chosen for mutation, is that the direction the pipeline is stretched to and how much it is stretched, is up to a point random. The chosen variable is moved a random number of grid points (up to a defined maximum) in a direction orthogonal to the adjacent portion of the pipeline. The mutation frequency of 0.1 was chosen by a method of trial and error.

3.3.4 Objective and penalty functions

There are three different objective functions employed in the second method of this study. For the Hverahlíð case study presented in chapter 4 the optimization is done first with regard to route length and visual effects and secondly with regards to pressure drop and visual effects. The pressure drop objective function is included as an optional part of the second method due to it possibly being beneficial to the design process to obtain and view the pareto front made up of visual effects and pressure drop. The final design could then conceivably take into account the trade-off between those two factors.

Visual effects

As previously stated, optimization of the visual effects of the pipeline is the main goal of this study. The NSGA II based method utilizes the distance transform visual effects ranking method presented in chapter 3.1 to provide the values of the visual effects of each pipeline. At the beginning of the algorithm the observation points/areas are discretized and the visual effects algorithm is run. The ranking matrix resulting from this is then used at every generation to calculate the visual effects objective function value. It should be noted that when the methods of this study are compared to each other, the resulting individuals have a different number of variables. For the first method the desired frequency of bends determines this number, which is then used for the comparison of the methods, as the pipeline resulting from the MLCDT algorithm is not really made up of a certain number of variables (or one variable for every grid point if looked at from another point of view).

Route length and incline

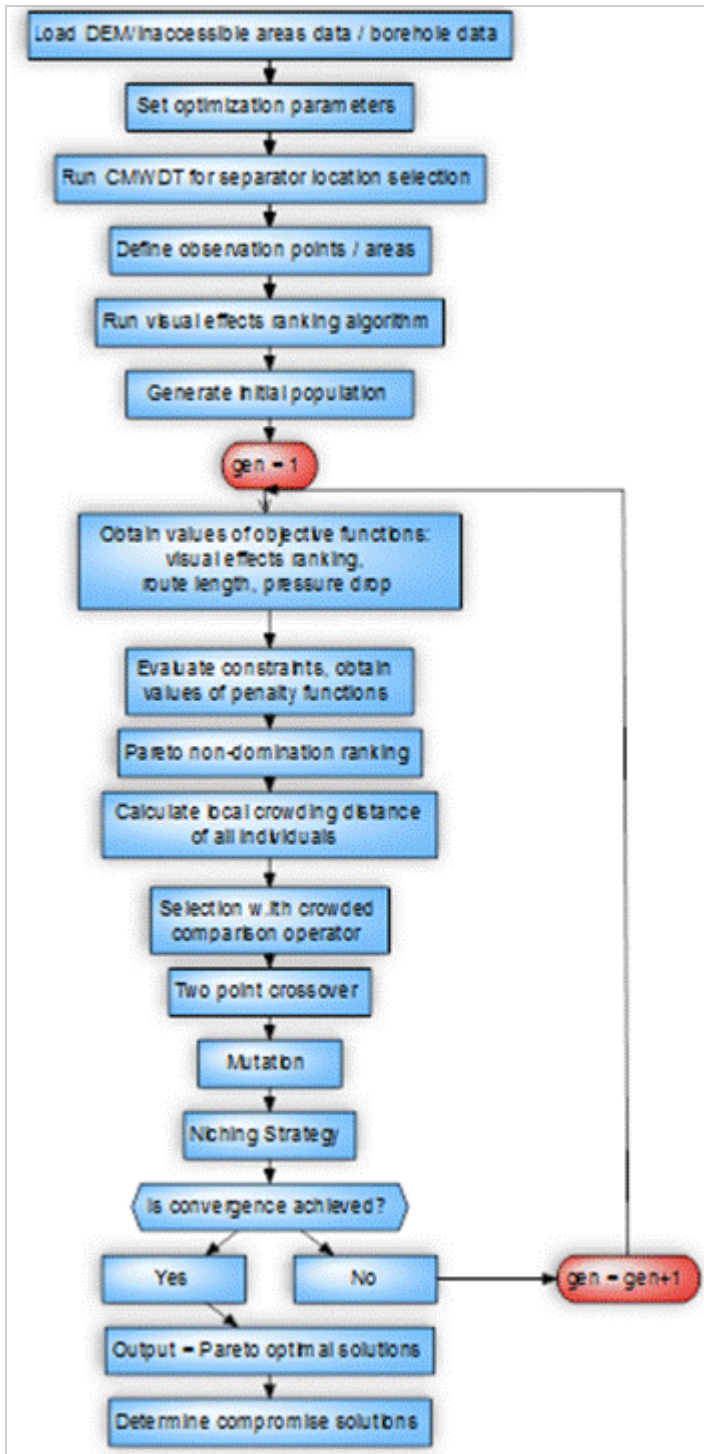
The most straightforward of the objective functions that the second method takes into account is the calculation of the route length. The distance between each variable of an individual to the adjacent variable is calculated and the route length is the sum of all the local distances between variables. As previously mentioned, in the geothermal industry today it is endeavored to design the pipeline routes monotonic with minimal incline in order to prevent slug flow conditions from forming in the pipeline. This is essentially incorporated and optimized in the first method of this study, the DT based method. For the second method of this study this is done in a similar way by keeping the route inclines in both directions under certain defined levels. A penalty function is included that draws down the route length objective function value if the defined maximum uphill or downhill gradients are exceeded.

Pressure drop

As mentioned in chapter 3.3.1, the use of GA's also offers the possibility of optimization with regards to minimizing the pressure drop in the pipeline (and therefore minimizing the drop in energy production). In the second method of this study pressure drop can be included as a special objective function in the NSGA II algorithm. The method uses the model presented in chapter 2.3 to calculate the pressure drop for each individual. As seen in chapter 2.3, for two different pipeline routes in the same geothermal area, with the same flow properties and the same start and end points, the total pressure drop will essentially be a function of the route length and the number of bends, expansion units and other installations. Therefore the route optimization with regards to first of visual effects and route length and second of all with regards to visual effects and pressure drop is not expected to result in very divergent routes. The benefit however, even though the objectives are similar, is to be able to use the pareto front of visual effects and pressure drop in the design process. The inclusion of this objective function is examined in chapter 4.6. It should be noted that optimization with regards to pressure drop was not the main goal of this study and is therefore included in only a part of the Hverahlíð case study.

Allowable area for each variable

The tolerance area defined by the initial population generation method presented in chapter 3.3.2 is used throughout the optimization at every generation. If the mutation operator causes a variable to move out of the defined tolerance area, the direction of mutation is simply reversed. F.a.e if the mutation caused the variable to move one grid point out of the tolerance area, instead it will move one grid point into the tolerance area. This is necessary to prevent the variables from overlapping and gathering in the same plausible areas.



Algorithm 4: Genetic algorithm based method

4 Results

For the purpose of estimating the effectiveness of the methods, they are implemented for the Hverahlíð geothermal area in Iceland. First of all in chapters 4.2-3 the NSGA II /DT and MLCDT methods will be implemented and in chapter 4.4 their results are compared to each other, the shortest route and the currently planned route. Subsequently in chapter 4.5 the addition of a random cost function to the MLCDT method is examined. Chapter 4.6 looks at the inclusion of the pressure drop objective function into the NSGA / DT method.

4.1 Geothermal area features and case study details

In figure 4.1 below is shown the preliminary plan for the Hverahlíð geothermal area in Iceland and figure 4.2 shows the corresponding digital elevation model. The shortest route through the proposed work area is used for comparison with the NSGA II / DT method and the MLCDT method. Matlab was used to implement the methods and for all calculations regarding the case study.

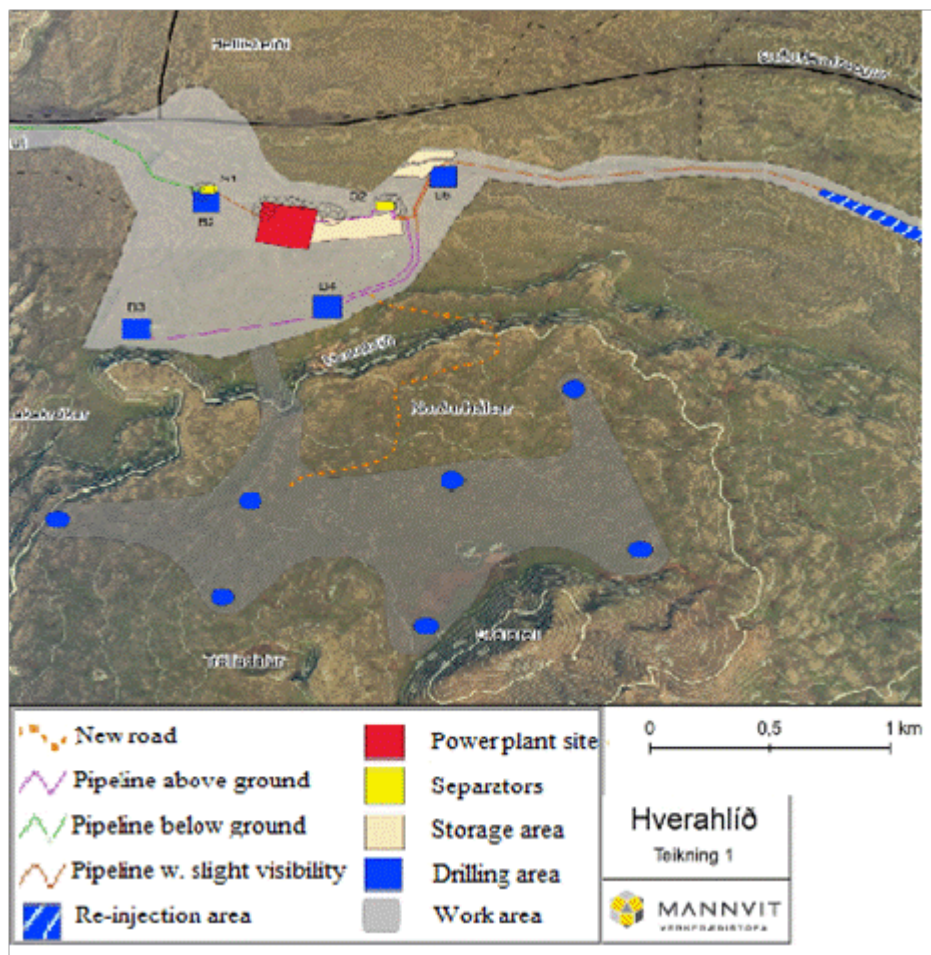


Figure 4.1: Preliminary plan by the power plant developers for the Hverahlíð geothermal area.

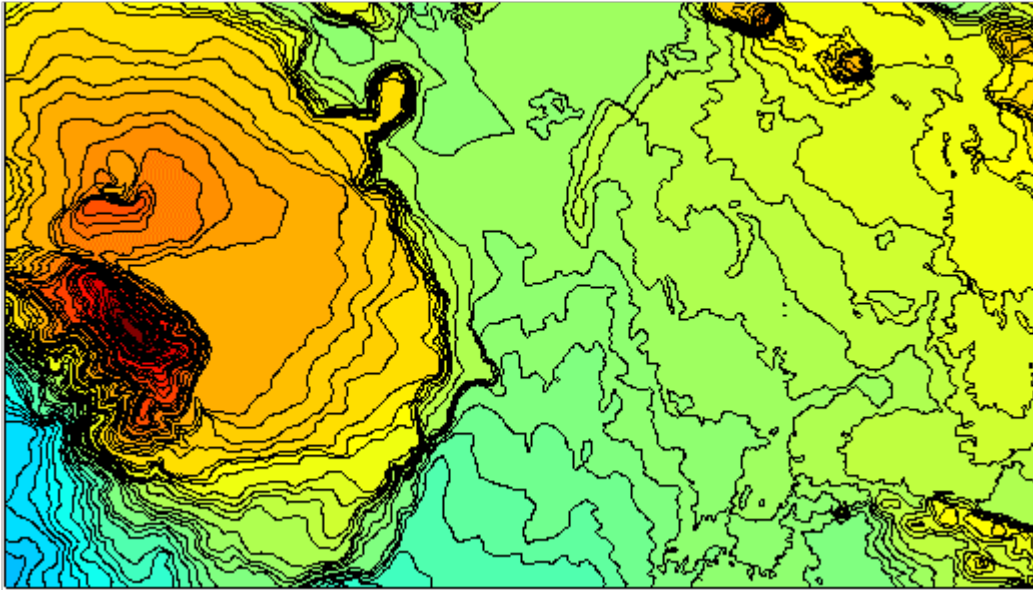


Figure 4.2: Digital elevation model representing the Hverahlíð geothermal area shown in figure 4.1. The scale is from blue – lowest altitude in the topography shown in figure 4.1 – to dark red – highest altitude in the topography shown in figure 4.1.

The problem as described by the company building and running the geothermal power plant at Hverahlíð, Reykjavík Energy (Orkuveita Reykjavíkur) is to obtain the optimal gathering point for all the pipelines from the boreholes on the upper platform and to then design the optimal route for the pipeline (with regards to visual effects and other factors), from the gathering point to the separator situated adjacent to the power plant area. The route incline constraints are maximum downward incline: 10% and upwards: 0%. To increase the difficulty of the problem (lengthen the route from gathering point to separator) only the three boreholes on the left on figure 4.1 are chosen for the pipeline gathering point selection. The pipeline gathering point chosen with the MWDT algorithm is displayed in all of the results as the start point for the pipelines.

4.2 Distance transform based method - results

In figure 4.3 below are displayed the results of the visual effects ranking method for the Hverahlíð geothermal area. As can be seen in the figure the most visible areas are clearly the hillsides between the upper and lower platforms, along with other hills and elevated areas that are highly visible. As can be seen in figure 4.3, the method is effective in ranking the topographical areas with regards to visual effects, as areas with low visibility, f.a.e valleys and areas behind elevated sites receive a low ranking in all cases. Highly visible areas also in all cases receive a high ranking.

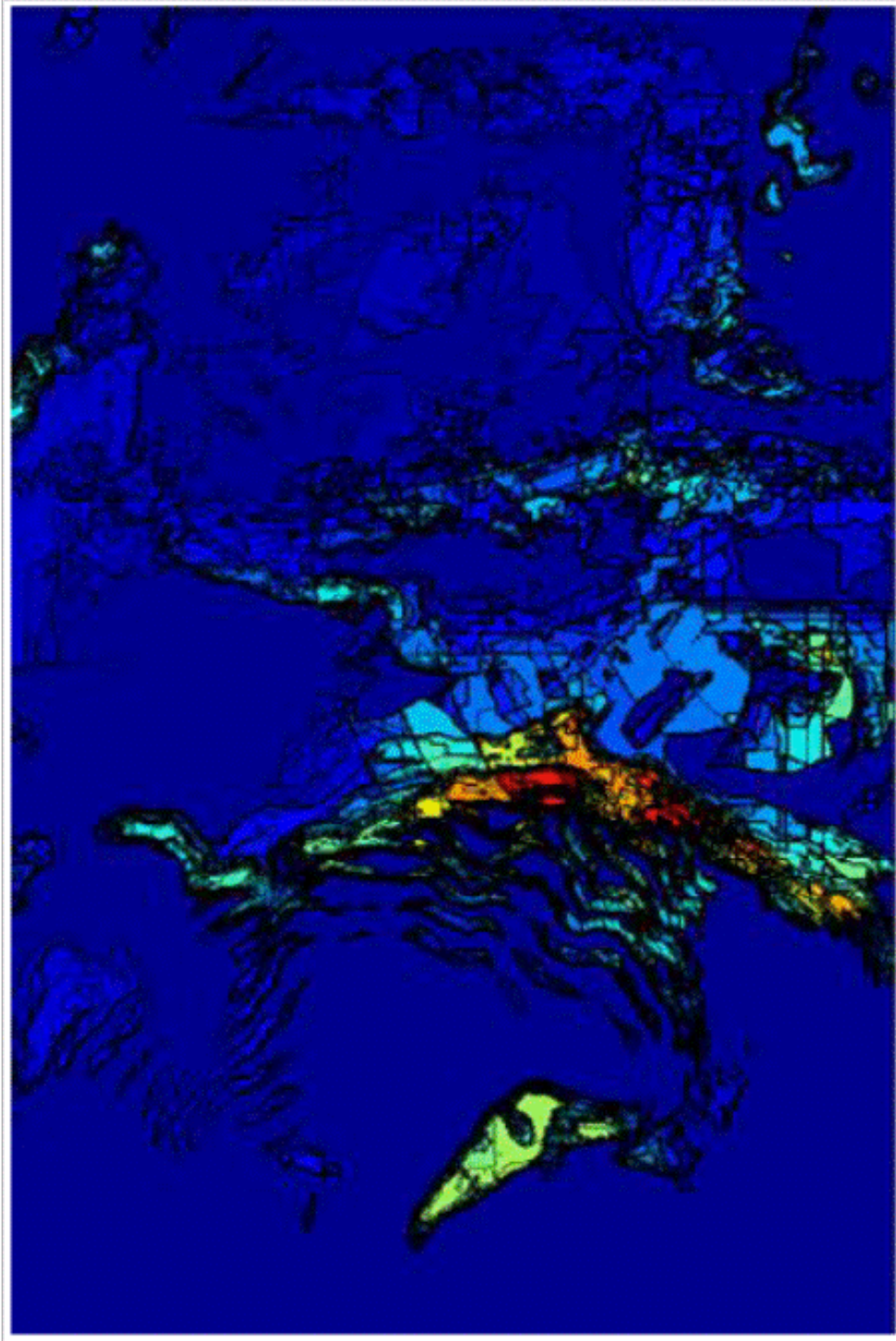


Figure 4.3: Hverahlíð visual effects ranking matrix obtained, using the visual effects ranking method presented in chapter 3.1, on the topography represented by the digital elevation matrix of the Hverahlíð geothermal area shown in figure 4.2. The scale is from dark blue – low visual effects ranking – to dark red – high visual effects ranking.

Figure 4.4.1 below displays the optimal route with regards to visual effects obtained using the MLCDT algorithm with only the visual effects ranking cost function. Figure 4.4.2 shows the route resulting from the GA modification to include expansion loops of the route in figure 4.4.1.

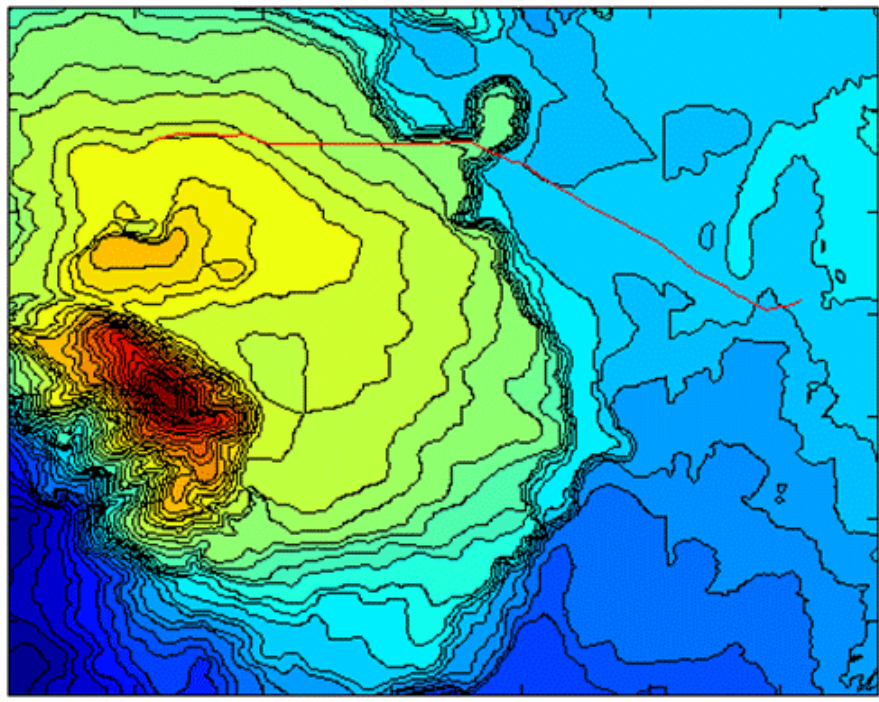


Figure 4.4.1: Digital elevation model of the Hverahlíð geothermal area and the optimal pipeline route, with regards to visual effects, obtained using the distance transform based method with regards to only visual effects. The red line represents the optimal visual effects route. The scale is from dark blue – lowest altitude – to dark red – highest altitude.

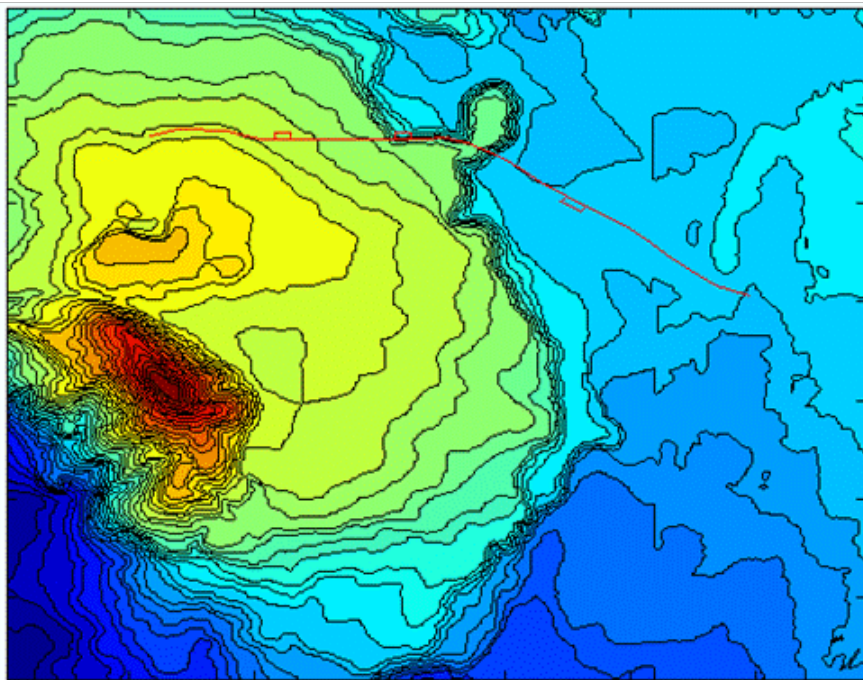


Figure 4.4.2: Digital elevation model of the Hverahlíð geothermal area and the genetic algorithm modified optimal pipeline route, with regards to visual effects, obtained using the distance transform based method with regards to only visual effects. The red line represents the optimal visual effects route with expansion loops. The scale is from dark blue – lowest altitude – to dark red – highest altitude.

As can be seen in figures 4.4.1-2 above, the chosen route takes a close to direct route to a valley, which provides cover from the observation areas. The incremental movements of the route vary considerably - the route in 4.4.1 includes a large number of bends. As described in chapter 3.2.3 the number of bends is then limited and expansion loops are included and their locations optimized, as shown in figure 4.4.2.

4.3 Genetic algorithm based method – results

For the second method an initial population of 100 individuals is chosen for the first run. The mutation rate used is 0.1 and the crossover rate is 0.9. The generated pipelines include 130 variables and in the DEM representation of the area there are approximately 115.000 points. The visual effects ranking matrix shown in figure 4.3 is used for the visual effects objective function. Figure 4.5 shows the first front obtained after 5000 generations. In the run displayed in figure 4.7 the population size has been increased to 200. Figure 4.6 shows four of the first front pipeline routes obtained using this method and figure 4.8 shows the GA modification of one of the routes in figure 4.8.

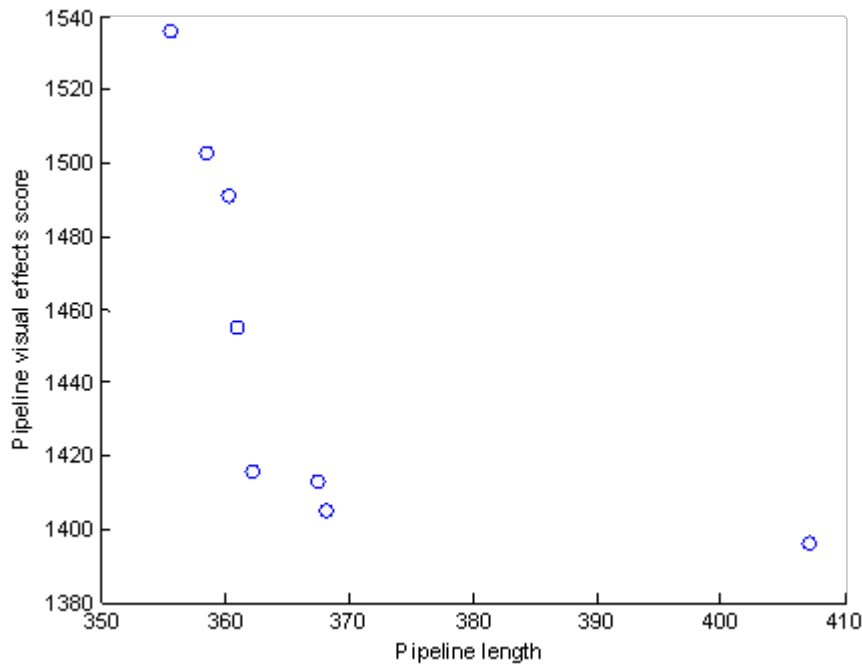


Figure 4.5: Objective function values of the first front in the pipeline population, generated using the genetic algorithm based method with the pipeline length and visual effects objective functions, after 5000 generations with a population size of 100 individuals. The first front individuals are indicated by the blue circles in the figure.

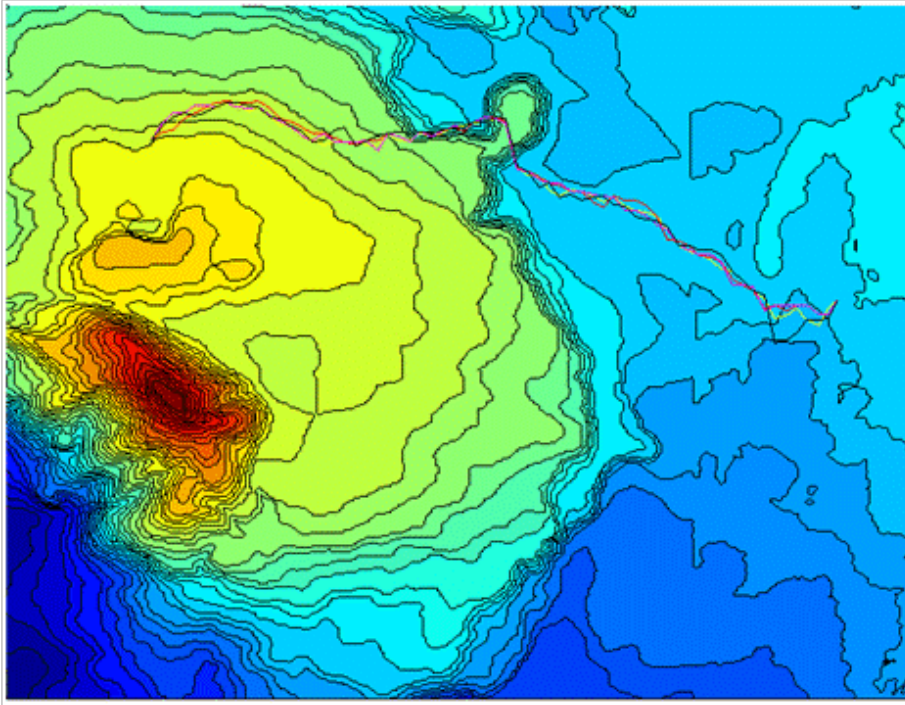


Figure 4.6: Digital elevation model of the Hverahlíð geothermal area and four first front routes generated using the genetic algorithm based method with regards to visual effects and pipeline length. The black, yellow, purple and red lines depict the first front routes. The scale is from dark blue – lowest altitude – to dark red – highest altitude.

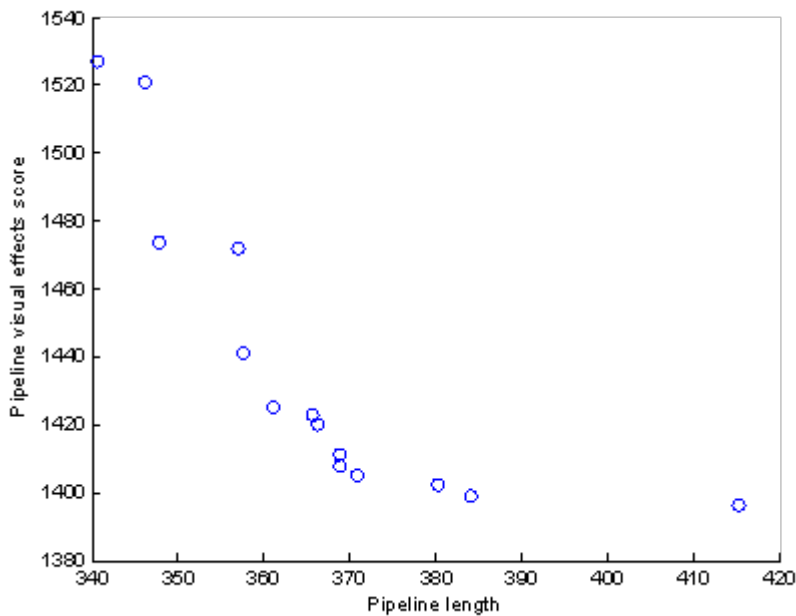


Figure 4.7: Objective function values of the first front in the pipeline population, generated using the genetic algorithm based method with the pipeline length and visual effects objective functions, after 5000 generations with a population size of 200 individuals. The first front individuals are indicated by the blue circles in the figure.

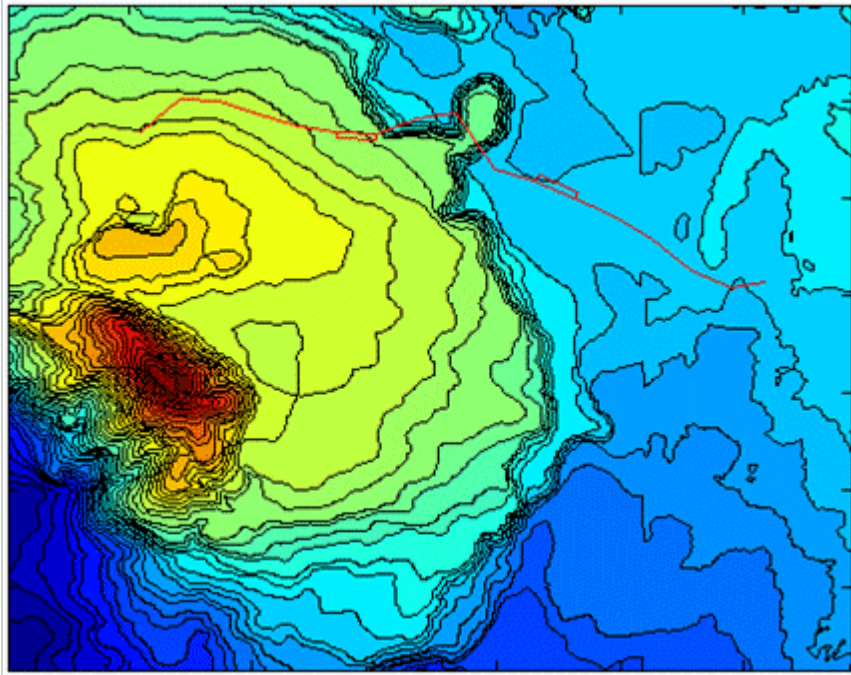


Figure 4.8: Digital elevation model of the Hverahlíð geothermal area and a first front route generated using the genetic algorithm based method with regards to visual effects and pipeline length, modified to include expansion loops. The red line depicts the first front route modified to include expansion loops. The scale is from dark blue – lowest altitude – to dark red – highest altitude.

4.4 Comparison of method performance

| Method | Length (DEM matrix units) – 6m | Visual impact ranking / point |
|----------------------------|--------------------------------|-------------------------------|
| MLCDT | 281 | 22.7 |
| NSGA II – pipe 1 | 340 | 23.5 |
| NSGA II – pipe 2 | 358 | 22.2 |
| NSGA II – pipe 3 | 368 | 21.7 |
| NSGA II – pipe 4 | 415 | 21.5 |
| Area plan – proposed route | 263 | 31.8 |

Table 1: Comparison of routes generated by the genetic algorithm and distance transform based methods

In table 1 above the visual impact ranking results are shown on a per-point basis. This is due the VTDT and NSGA II routes having a different number of varying points. As can be seen in table 1 the VTDT route performs better than all the NSGA II routes. It has a lower visual effects ranking than the NSGA II routes (1st, 5th, 9th and 14th routes from the second NSGA II run, from the left in figure 4.6). It is also significantly shorter. This could result from there not being enough variables in the NSGA II optimization or the multitude of possible routes can be preventing the NSGA II method from obtaining the true pareto optimal front, indeed as figures 4.5 and 4.7 show the obtained front is not truly pareto optimal.

4.5 MLCDT with and additional cost function

To examine the ability of the MLCDT algorithm to handle multiple cost functions, a different gathering point (than in the previous part of the case study) is chosen and the algorithm run first of all with only the visual effects cost function and secondly with an added cost function. The second cost function is essentially a randomly generated matrix of the same size as the visual effect ranking matrix. The reason for using a randomly generated matrix is to examine whether the optimization will result in a different optimal route.

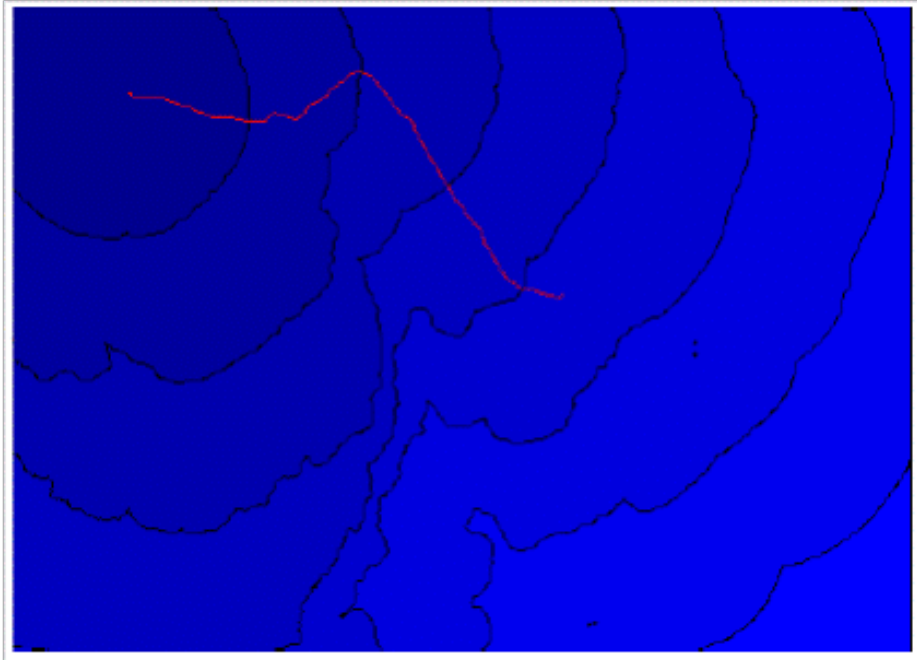


Figure 4.9.1: Visual effects isolines and optimal route at Hverahlíð, generated using the distance transform based method with regards to only the visual effects objective function. The red line depicts the optimal route and the scale is from dark blue – lowest value of the resulting VTDT matrix - to light blue– highest value of the resulting VTDT matrix.

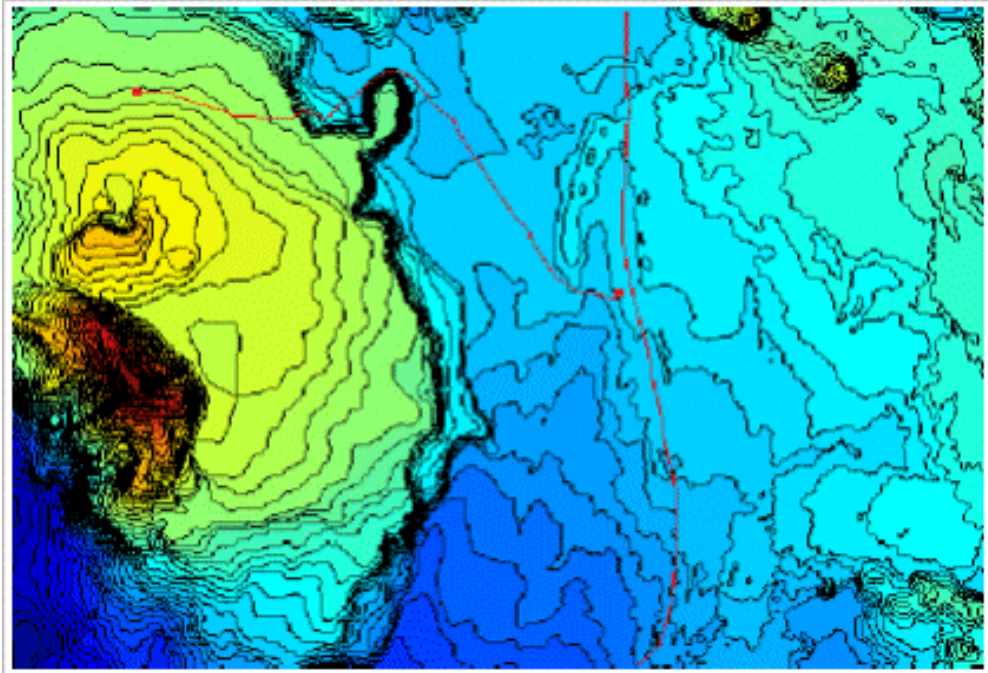


Figure 4.9.2: Digital elevation model of the Hverahlíð geothermal area and optimal route at Hverahlíð generated using the distance transform based method with regards to only the visual effects objective function. The left red line depicts the optimal route and the right vertical red line depicts the road defined as the observation area. The scale is from dark blue – lowest altitude – to dark red – highest altitude.

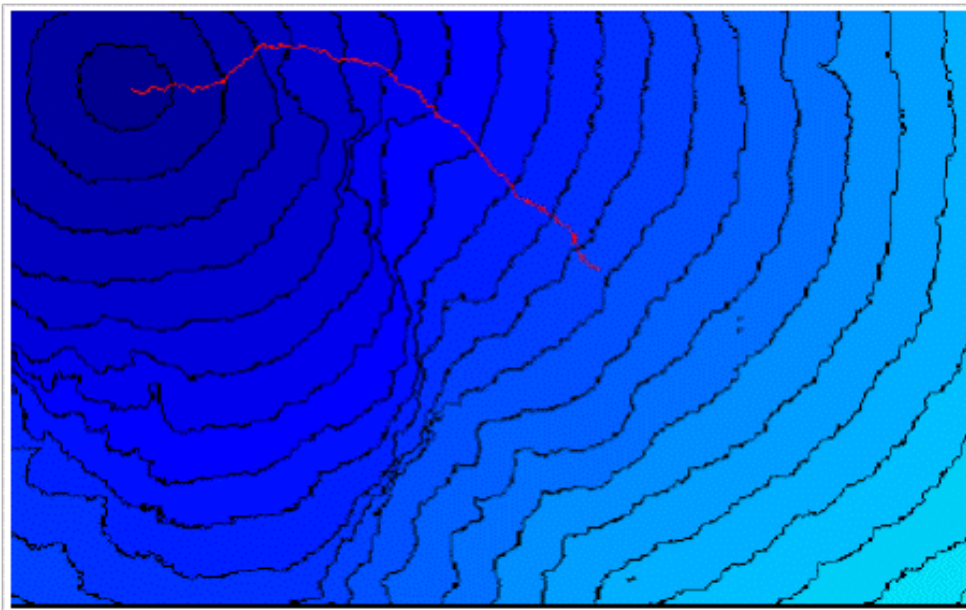


Figure 4.10.1: Visual effects isolines and optimal route at Hverahlíð, generated using the distance transform based method with regards to both the visual effects and random objective functions. The red line depicts the optimal route and the scale is from dark blue – lowest value of the resulting VTDT matrix - to light blue– highest value of the resulting VTDT matrix.

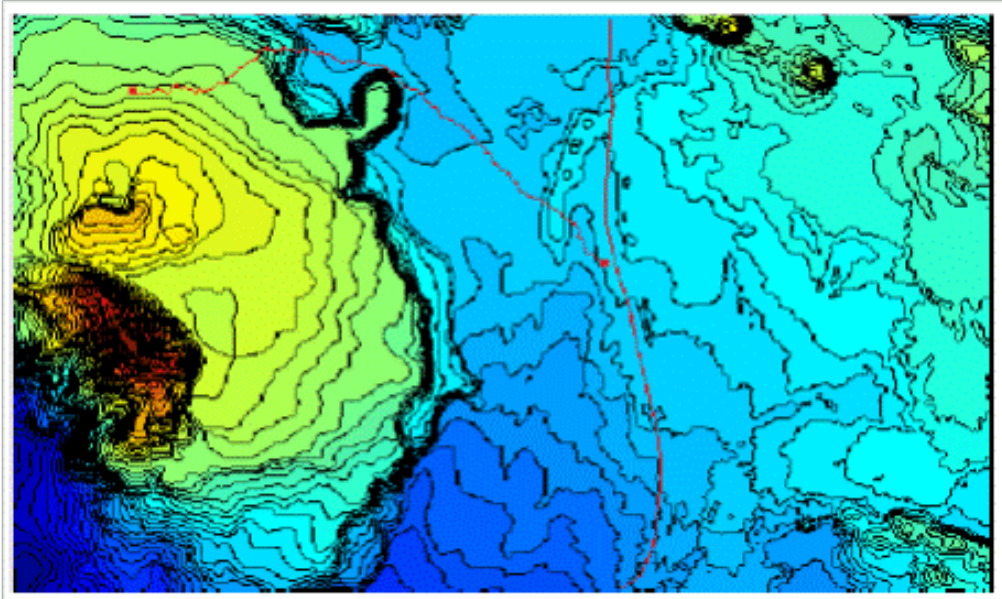


Figure 4.10.2: Digital elevation model of the Hverahlíð geothermal area and optimal route at Hverahlíð generated using the distance transform based method with regards to both the visual effects and random objective functions. The left red line depicts the optimal route and the right vertical red line depicts the road defined as the observation area. The scale is from dark blue – lowest altitude – to dark red – highest altitude.

Figures 4.9.1-2 and 4.10.1-2 above show that the inclusion of an additional random cost function has significantly altered the route in some areas. Upon closer inspection the majority of the route shifts by at least one grid point, this is due to effect of the second cost function, which even though it is random and therefore not expected to alter the route radically, shifts the results of repeated applications of equations 3.2-3 when applying a mask to a grid point.

4.6 Inclusion of a pressure drop objective function

In order to examine the inclusion of a pressure drop objective function in the based method, a theoretical example is set up (not reflecting the conditions at Hverahlíð). Table 2 shows the parameters used in the implementation of the GA based method for this example. The respective start and end points of the routes are the same as for the main part of the case study in chapters 4.1-5. Note that the purpose of this example is not to accurately predict the pressure drop of the pipelines at Hverahlíð, rather to theoretically examine the inclusion of the pressure drop objective function in the GA based method

| | |
|---|--------|
| T | 150°C |
| x | 0,3 |
| d | 0,4m |
| m | 40kg/s |

Table 2: Conditions for pressure drop calculations example

Using equation 2.18 the calculated void fraction is 0,87. The calculated static pressure gain, due to the lower altitude of the separator location than the pipeline start point, is 0,89 bars. This explains why the total pressure drop of the pareto optimal routes ranges from -70 to 60 mbar, as shown in figure 4.12. Figure 4.11 below shows three of the recommended routes (numbers 1, 5 and 9 from the left in figure 4.12). The routes are all very similar to the routes shown in figure 4.6. This is, as was covered in chapter 3.3.3, expected due to the pressure drop being for the most part a function of the total pipeline length.

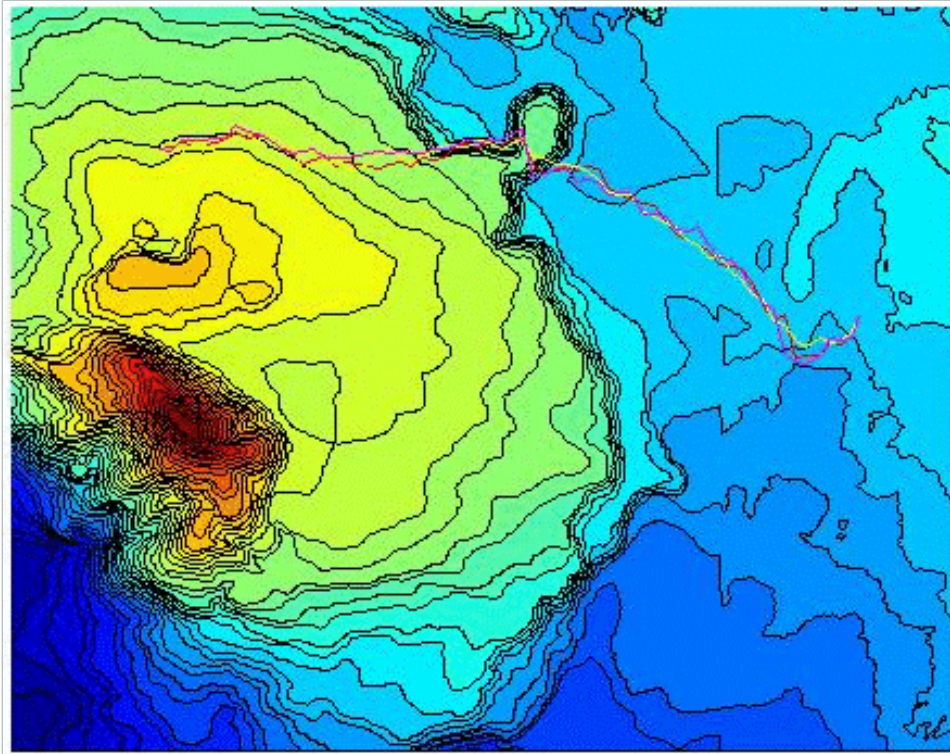


Figure 4.11: Digital elevation model of the Hverahlíð geothermal area and three first front routes generated using the genetic algorithm based method with regards to visual effects and pressure drop. The yellow, purple and red lines depict the first front routes. The scale is from dark blue – lowest altitude – to dark red – highest altitude.

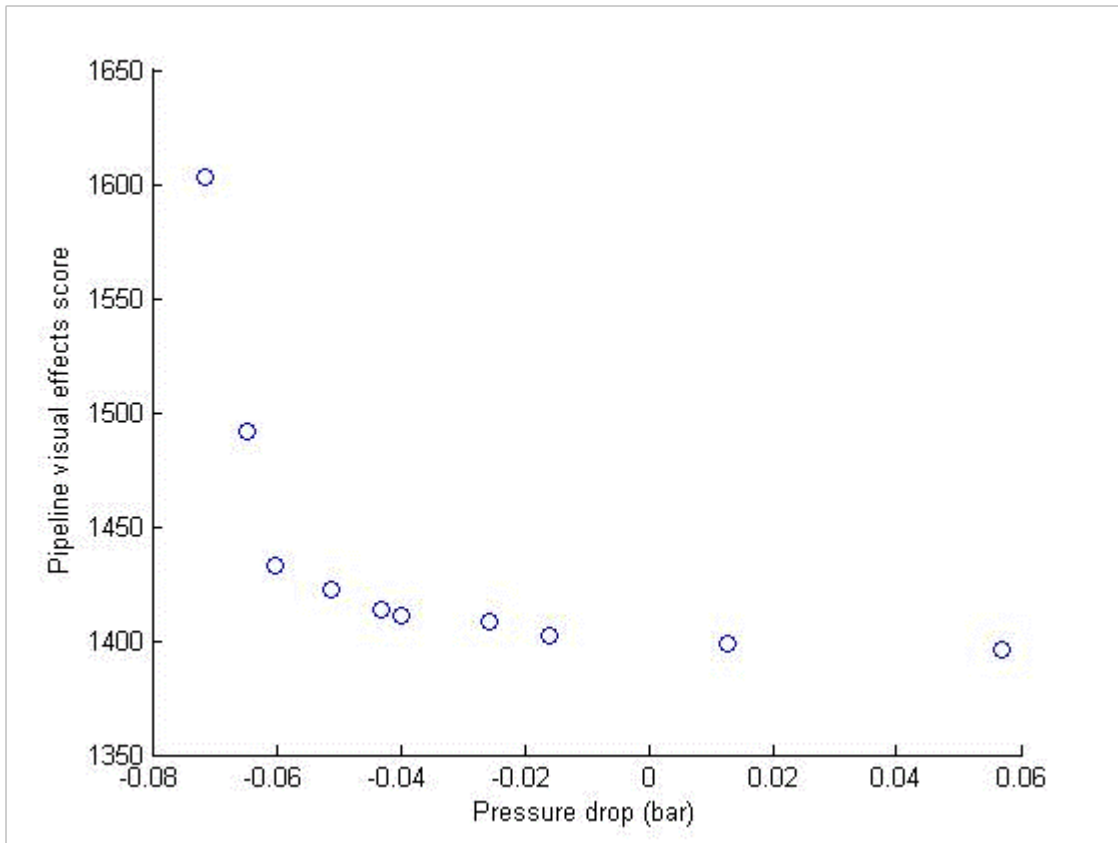


Figure 4.12: Objective function values of the first front in the pipeline population, generated using the genetic algorithm based method with the pipeline length and pressure drop objective functions, after 5000 generations with a population size of 200 individuals. The first front individuals are indicated by the blue circles in the figure.

5 Conclusions and future work

The case study presented above shows that both the methods presented by this study are effective in obtaining pipeline routes with significantly less visual effects than conventionally designed pipeline routes. The distance transform based method used in this study and the visual effects ranking system introduced offer a good, functional way to design pipeline routes with regards to minimal visual impact while also keeping the route length reasonable. The results show that both methods are successful in designing a route minimizing the visual impact of a pipeline while meeting design constraints. This is shown well in how the method differs from and performs better than the route originally proposed by the Hverahlíð geothermal area planners. Using the DT based method, there is virtually no upper limit on the level of detail achievable designing the optimal route. The only limit is that of the resolution of the DEM used.

The genetic algorithm based method performs worse than the distance transform based method and this indicates that the pareto front obtained by the GA based method is not the “true” pareto optimal front, but the method is however promising due to the possibility of including further cost functions. The MLCDT algorithm requires further work to be able to optimize with regards to more than one cost function. The addition of expansion loops was successfully optimized after the route optimization in both methods. Proposed future work in the development of this method is to include the expansion loop sites and geometry as variables in the NSGA II optimization. The MLCDT algorithm needs further work to be able to better handle multiple cost functions.

References

- Arora, J. (2004). *Introduction to optimum design*. Elsevier.
- Azzi, A., Friedel, L., & Belaadi, S. (2000). Two-phase gas/liiquid flow pressure loss in bends. *Forschung im Ingenieurwesen* 65 (bls. 309-318). Springer-Verlag.
- Bell, J., & McMullen, P. (2004). Ant colony optimization techniques for the vehicle routing problem. *Advanced Engineering Informatics* 18 (bls. 41-48). Elsevier.
- Borgefors, G. (1986). Distance transformations in digital images. *Computer Vision, Graphics and Image processing* 34, 344-371.
- Butt, M., & Maragos, P. (1996). *Optimal design of chamfer distance transforms*. Atlanta, GA: Georgia Institute of Technology.
- Cheng, F., & Li, D. (1995). *Genetic algorithm developement for multiobjective of structures*. Rolla: University of Missouri .
- Chexal, B., Horowitz, J., McCarthy, G., Merilo, M., & Sursock, J. (1999). *Two-phase pressure drop - Technology for design and analysis*. Palo Alto, CA: EPRI.
- Chisholm, D. (1979). Two-phase flow in bends. *International Journal of Multiphase Flow* 6, (bls. 363-367).
- Deb, K., & Goldberg, D. (1989). An investigation of niche and species formation in genetic function optimization. *Proceedings of the 3rd International Conference on Genetic Algorithms*, (bls. 42-50).
- Deb, K., Agrawal, S., Pratap, A., & Meyarivan, T. (2002). *A fast elitist non-dominated sorting genetic algorithm for multi-objective optimization: NSGA-II*. Kanpur: Kanpur Genetic Algorithms Laboratory.
- Gass, S. (1985). *Linear programming: Methods and applications*. Courier Dover Publications.
- Geem, Z., Lee, K., & Park, Y. (2005). Application of harmony search to vehicle routing. *American Journal of Applied Sciences* 2 (12) (bls. 1552-1557). Science Publications.
- Goldberg, D. (1989). *Genetic algorithms in search, optimization and machine learning*. Reading, MA: Addison-Wesley.
- Gopalakrishnan, T., & Sooda, K. (2009). Comparison of genetic algorithm and simulated annealing technique for optimal path selection in network routing. *National Conference on VLSI and Networks*, (bls. 47-53). Chennai.

- Harrison, R. (1975). *Method for the analysis of geothermal two-phase flow*. The University of Auckland.
- Haubt, R., & Haubt, S. (2004). *Practical genetic algorithms*. Hoboken, New Jersey: John Wiley & Sons.
- Jónsson, M. (2010). *Transportation systems*. Reykjavík: University of Iceland.
- Kjaernested, S., Jonsson, M., & Palsson, H. (2011). A methodology for geothermal pipeline route selection using distance transform algorithms. *Stanford Geothermal Congress*. Palo Alto, CA.
- Kristinsson, H. (2005). *Pipe route design using variable topography distance transforms*. Reykjavík: University of Iceland.
- Leymarie, F., & Levine, M. (1992). A note on "Fast raster scan distance propagation on the discrete rectangular lattice". *Computer Vision and Image Understanding*, Vol. 55, No. 1, (bls. 84-94).
- Pálson, H., Bergþórson, E., & Pálson, O. (2006). Estimation and validation of models of two phase flow from geothermal wells. *10th International Symposium on District Heating and Cooling*, (bls. Sektion 5a - Renewable energy and district heating).
- Reykjavíkurborg, O. (2010). Information on Hverahlíð geothermal area, images, planning information, DEM, contour files.
- Rosenfeld, A., & Pfaltz, J. (1968). Distance functions on digital pictures. *Pattern Recognition*, Vol 1, 33-61.
- Smith, M. (2004). Distance transform as a new tool in spatial analysis, urban planning and GIS. *Environment and planning B: Planning and design*, Vol 31, 85-104.
- Smith, M. (2005). *Determination of gradient and curvature constrained optimal paths*. London: University College .
- Srinivas, N., & Deb, K. (1995). Multiobjective optimization using non-dominated sorting in genetic algorithms. *Evolutionary Computation* 2, 221-248.
- Thome, J. (2006). *Engineering data book III*. Lausanne, Switzerland: Wolverine Tube inc.
- Woldesemayat, M., & Ghajar, A. (2007). Comparison of void fraction correlations for different flow patterns in horizontal and upward inclined pipes. *International Journal of Multiphase Flow* 33, 347-370.
- Wood, C. (2008). Sótt 2010 frá Cover image: <http://corey-wood.com>
- Yavuz, K. (2004). *Multi-objective mission route planning using particle swarm optimization*. Air Force Institute of Technology.
- Zhao, H., Lee, K., & Freeston, D. (2000). Geothermal two-phase flow in horizontal pipes. *Proceedings World Geothermal Congress*, (bls. 3349-3353). Kyushu-Tohoku.

